Physics        College of Arts and Sciences

# The Three-Dimensional Random Field Ising Magnet: Interfaces, Scaling, and the Nature of States

Alan Middleton
*Syracuse University*

Daniel S. Fisher
*Harvard University*

# The three-dimensional random field Ising magnet: interfaces, scaling, and the nature of states

A. Alan Middleton

*Department of Physics, Syracuse University, Syracuse, New York 13244*

Daniel S. Fisher

*Lyman Laboratory of Physics, Harvard University, Cambridge, Massachusetts 02138*

(Dated: February 1, 2008)

The nature of the zero temperature ordering transition in the three dimensional Gaussian random field Ising magnet is studied numerically, aided by scaling analyses. Various numerical calculations are used to consistently infer the location of the transition to a high precision. A variety of boundary conditions are imposed on large samples to study the order of the transition and the number of states in the large volume limit. In the ferromagnetic phase, where the domain walls have fractal dimension $d_s = 2$, the scaling of the roughness of the domain walls, $w \sim L^\zeta$, is consistent with the theoretical prediction $\zeta = 2/3$. As the randomness is increased through the transition, the probability distribution of the interfacial tension of domain walls scales in a manner that is clearly consistent with a single second order transition. At the critical point, the fractal dimensions of domain walls and the fractal dimension of the outer surface of spin clusters are investigated: there are at least two distinct physically important fractal dimensions that describe domain walls. These dimensions are argued to be related by scaling to combinations of the energy scaling exponent, $\theta$, which determines the violation of hyperscaling, the correlation length exponent $\nu$, and the magnetization exponent $\beta$. The value $\beta = 0.017 \pm 0.005$ computed from finite size scaling of the magnetization is very nearly zero: this estimate is supported by the study of the spin cluster size distribution at criticality. The variation of configurations in the interior of a sample with boundary conditions is consistent with the hypothesis that there is a single transition separating the disordered phase with one ground state from the ordered phase with two ground states. The array of results, including values for several exponents, are shown to be consistent with a scaling picture and a geometric description of the influence of boundary conditions on the spins. The details of the algorithm used and its implementation are also described.

## I. INTRODUCTION

In spite of many years of study, the behavior of phases and phase transitions that are dominated by quenched randomness is still controversial. One such lively controversy has concerned the existence or lack thereof of an ordered phase in the random field Ising model (RFIM) in three dimensions. Although this was eventually resolved in the affirmative by rigorous work,[1] the nature of the phase transition and the possibility of a phase intermediate between the paramagnet and the ferromagnet is still controversial.

Numerical simulations of the random field Ising model — and experiments — are impeded by the dramatic slowing down that occurs as the phase transition is approached due to the existence of free energy barriers which are broadly distributed but typically grow as a power of the correlation length. Such barriers are general characteristics of phases controlled, in a renormalization group (RG) sense, by stable zero temperature fixed points. For the random field Ising model, not only is the low temperature phase controlled by a zero-temperature fixed point (as is the case for conventional pure systems), but the phase transition itself is also controlled by such a fixed point.[2,3] Indeed, the ground state properties of the random field Ising model undergo a phase transition as the strength of the randomness is increased and it is this

zero-temperature transition that governs the behavior of the transition at positive temperatures. Fortunately, this means that much can be learned by studying the ground state properties.

It has been known for some time that combinatorial algorithms can be used effectively to find the ground states of various classes of random systems and the RFIM was one of the first to be studied in this way.[4] With current computers, the algorithm is very fast and large system sizes can be studied in enough detail to obtain good statistics enabling the tools of finite size scaling to be used to analyze the zero-temperature phase transition.

Various significant open questions exist about the phase transition in the RFIM. Although a self-consistent scaling picture of a zero-temperature critical fixed point was proposed early on, it has not been adequately tested and other scenarios have been suggested, including a first order phase transition[5,6] and an intermediate phase with "replica-symmetry breaking"[7,8] presumably meaning many coexisting equilibrium states.

In this paper we study the RFIM with Gaussian distributed random fields, focusing on the nature of the phase transition and the sensitivity of the ground states to varying boundary conditions (BCs) as a probe of the number and nature of the infinite system states. As will be explained in some detail, our results strongly support the scaling picture of the transition. In this picture, there is a single second order critical point characterized by

three scaling exponents: $\nu$ for deviations from the critical point, $\theta$ for the energy at the critical point, and $\beta/\nu$ for the magnetization at the critical point. We clarify some of the substantial confusion about the order of the transition by showing that both $\theta$ and $\nu$ as well as the distributions of the "stiffness" and spin clusters are very different from what they would be at a first order transition. Nevertheless, as observed previously, the magnetization exponent $\beta$ is extremely small so that even with the very large sizes we study, the magnetization appears almost discontinuous.

## II. MODEL AND NUMERICAL METHOD

The random field Ising model[9] has Hamiltonian, defined over spin configurations $\{s_i = \pm 1\}$,

$$H = -J \sum_{\langle ij \rangle} s_i s_j - \sum_i h_i s_i, \qquad (1)$$

with the random fields $h_i$ chosen independently from a distribution which we take to be Gaussian with mean zero and variance $h^2$. The ferromagnetic exchange coupling, $J$, is fixed at unity in the simulations and the sites $i$ lie on a cubic lattice with interactions between nearest neighbor pairs $\{\langle ij \rangle\}$. The basic nature of the phase diagram of the 3-D RFIM is well-known: As the temperature is lowered for small $h$, there will be a critical temperature, $T_c(h)$, below which the RFIM becomes ferromagnetically ordered with a non-zero spontaneous magnetization. As the strength of the random field increases, the critical temperature decreases until at a critical field, $h_c$, it goes to zero.

Both the paramagnetic and the ferromagnetic phases have been proven to exist at both zero and positive temperatures[1] and the transition between them can thus be studied by varying $h$ at $T = 0$. The simplest scenario at zero-temperature is a single critical field strength $h_c$ above which the spins are disordered with a unique infinite-system ground state and exponential decay of correlations, and below which there are two infinite-system ground states, one with predominantly up spins and the other with predominantly down spins.

The nature of the phases and the phase transition(s) between them can be probed by studying the effects of various boundary conditions on larger and larger systems — most simply cubes of size $\mathcal{V} = L \times L \times L$. In the disordered phase the orientation of a spin far from the boundaries is typically determined by the collection of random fields within a correlation length $\xi(h)$ of the spin and is insensitive to boundary conditions imposed far away. In contrast, in the ferromagnetic phase some spins will still be controlled by the random fields in their vicinity, but a finite fraction of the spins will be controlled by the boundary conditions — no matter how far away they are imposed. The simplest scenario is a single transition between these two phases. The primary goal of this paper is

to examine in detail the nature of this zero-temperature phase transition.

Many previous studies of the ground states of the RFIM (as well as finite temperature studies) have focused on the magnetization per spin, $m = \mathcal{V}^{-1} \sum_i s_i$, and the results have been somewhat ambiguous. Some have interpreted the numerical results as indicating a second order transition,[4,10,11] while others have concluded that the transition is first order.[6] Some Monte Carlo results[12] suggest that the finite-temperature transition is second order, but with the magnetization exponent $\beta$ nearly zero. Others,[13] using a varying external field, have found a coexistence of states suggestive of a first order transition. It is clear from these studies that if the transition is second order, the order parameter exponent $\beta$, $|m| \sim (h_c - h)^\beta$ must be very small, making definitive conclusions based on magnetization alone difficult. We have thus focused much of our attention — particularly for locating the transition and finding the exponents — on other properties which naturally distinguish the phases.

### A. Algorithm

The (almost surely) unique ground state of a finite sample can be determined in time polynomial in the number of spins.[14] The method is based on a reduction of the problem of determining RFIM ground states to a maximum-flow problem on an augmented graph. One can then use combinatorial optimization algorithms[15,16,17,18] to solve the maximum-flow problem. We describe the special features of the algorithm implementation, its verification, sample timings, and the use of integer valued $h_i$ in the Appendix.

### B. Statistics and analysis

We have studied system sizes up to $256^3$, which contain over $1.6 \times 10^7$ spins. Independent samples were simulated for each value of $h$. Separate realizations were also generated for boundary induced domain walls, spin cluster properties, magnetization, and the thermodynamic limit studies. The same samples and domain walls were used in the stiffness and domain wall property studies. For smaller systems ($8^3$ through $32^3$), $10^5$ samples were optimized, typically. (For the domain roughness measurements in the ordered phase, $10^2$ or $10^3$ samples provided sufficient data, as fluctuations in the interface width are not large.) Of order $10^3$ to $10^4$ samples were studied for each quantity for the $64^3$ and $128^3$ samples. For $L = 256$, $4 \times 10^2$ to $10^3$ samples were studied at each $h$, as part of the magnetization and cluster studies.

Error bars for exponent values throughout this paper include both estimated systematic errors due to apparent finite size effects and errors due to statistical uncertainties; the error bars represent an estimated range of values in which the value lies, with high confidence. In

contrast, error bars in the figures reflect $1\sigma$ statistical uncertainties, which we find to be generally consistent with confidence intervals found by resampling.

Generally (except for the stiffness, the roughness in the ferromagnetic phase, fitting a power law to the bond energy density, and the $P_{D/O,\pm}$ plots), we have used estimates of effective exponents as a function of system size to estimate exponents, rather than scaling plots. This is done to more clearly see trends in the data that reflect finite size corrections. Finite size corrections tend to be monotonic and introduce a drift with $L$ in the effective exponents. Given the good statistics of the data sets that can be generated with optimization algorithms, collapsing data can obscure these corrections, as the drift can be corrected with a slightly erroneous exponent. Where we have used scaling plots, we do not try to collapse all of the data onto a single curve, but keep in mind that the finite size corrections give a consistent drift with system size and we therefore tried to optimize the fit to the largest systems and near $h_c$.

## III.   SUMMARY OF RESULTS

As we are interested in the behavior of the RFIM in the thermodynamic limit, we have studied the approach to the infinite-volume limit using finite-size scaling analysis techniques similar to those applied to spin glasses and other random systems.[19,20,21,22,23,24] However, in contrast with ground state studies of spin glasses and other random models for which only a single thermodynamic phase exists, the results presented here give insight into the transition between two phases.[25]

### A.   Stiffness

The fundamental difference between an ordered phase and a disordered one is the *stiffness* (or rigidity) of the former: the free energy cost of changing one part of a system with respect to another part far away. At a macroscopic level, this free energy cost must be at least of order $k_B T$ and is usually much larger, diverging as a power of the system size. For an Ising ferromagnet, this stiffness is provided by the free energy cost of a domain wall which scales as its surface area. Thus a natural quantity to study for the ground states of the RFIM is the domain wall energy. This can be obtained from the difference in energy between antiparallel and parallel boundary conditions imposed on opposite sides of a system of cross sectional area $L^2$. A particular combination of these we call the *stiffness*, which we denote by $\Sigma$. Because of the randomness, this energy will be sample dependent and there is information to be gleaned from its distribution as well as its mean.

The scaling theory of the putative critical point of the random field Ising model predicts that the distribution of the stiffness will have a scaling form near the critical point:

$$\text{Prob}[d\Sigma] \approx \frac{d\Sigma}{CL^\theta} P\left(\frac{\Sigma}{CL^\theta}, K(h - h_c)L^{1/\nu}\right) \quad (2)$$

with $\theta$ and $\nu$ universal exponents, $P$ a universal scaling function (which does, however, depend on the shape of the sample), and $C$ and $K$ non-universal coefficients. In the *ferromagnetic phase*, the distribution of the stiffness will be sharply peaked at long length scales about a mean value which grows as $\sigma(h)L^2$ with $\sigma(h)$ the interfacial tension. This interfacial tension vanishes as $h \nearrow h_c$. In the *disordered phase*, $\Sigma$ will typically fall off exponentially for system thicknesses, $L$, much larger than the correlation length $\xi(h) \sim (h - h_c)^{-\nu}$. This exponential decay of the stiffness with $L$ is confirmed for all values $h > h_c$ examined in our numerical results.

At the *critical point*, the distribution of $\Sigma$ will be broad with both mean and width of order $L^\theta$. The exponent $\theta$ thus characterizes the scaling of the stiffness at the critical point. As long as $\theta$ is positive, the basic features of the zero-temperature critical point will be stable to thermal fluctuations and the finite-temperature transition will be in the same universality class.[2]

Our studies of the stiffness are based on computing energies for samples periodic in two directions and having fixed uniform boundary spins on the other two faces. Our results are very consistent with the scaling predictions for the larger system sizes, up to $128^3$, close to the critical point, which occurs at

$$h_c \simeq 2.270 \pm 0.004. \quad (3)$$

This location for the critical point is consistent with those obtained from scaling analyses of the domain wall dimension and the magnetization. It is somewhat lower than some previously reported estimates such as $h_c \approx 2.33$,[4,10] but it is consistent with the values $h_c = 2.29 \pm 0.04$ reported by Hartmann and Nowak[11], $h_c = 2.26 \pm 0.01$ reported by d'Auriac and Sourlas,[5] and $h_c = 2.28 \pm 0.01$ reported by Hartmann and Young.[26] Taking $h_c = 2.270$, the exponents that give a good scaling fit for the stiffness are found to be

$$\theta \simeq 1.49 \pm 0.03 \quad (4)$$

and

$$\nu \simeq 1.37 \pm 0.09. \quad (5)$$

The value for $\theta$ is consistent with exact bounds as well as with values derived from finite temperature simulations by applying exponent relations to measured critical behavior.[12] Note that if the transition had been first order, one would have expected to find $\theta = d - 1 = 2$, with a double peaked distribution of $\Sigma$ corresponding to "ordered" and "disordered" samples, and an effective $\nu = 2/d = 2/3$; the results we find are far from these.

From the modified hyperscaling law appropriate to transitions governed by zero temperature fixed points,[2,3]

$$(d - \theta)\nu = 2 - \alpha \quad (6)$$

with $d$ the dimension, here equal to three, we predict that the specific heat exponent for the finite-temperature transition (and for the second derivative of the energy with respect to $h$ at zero-temperature near the transition) is

$$\alpha = 2 - (3 - \theta)\nu \simeq -0.07 \pm 0.17. \qquad (7)$$

We also fit the sample averaged bond part of the energy, $\overline{E}_J$, at $h_c$ to the form $\overline{E}_J \sim c_1 - c_2 L^{(\alpha-1)/\nu}$ to more directly obtain $\alpha$, inspired by the recent approach of Hartmann and Young,[26] who examined the scaling of the derivative $dE_J/dh$. We find a consistent value for $\alpha$ using similar methods, although our value disagrees substantially with that of Hartmann and Young. We also use an extrapolation of $\overline{E}_J$, based on the dimension of the domain wall surfaces, which define $E_J$, to find

$$\alpha = -0.01 \pm 0.09. \qquad (8)$$

Both values are consistent with experiments,[27] which yield a small value of $\alpha$.

### B. Domain walls

In addition to the stiffness measurements, we have investigated the properties of the domain walls that are forced by appropriate changes of the boundary conditions. In the ferromagnetic phase, we expect that these will be flat on large length scales and have area proportional to $L^2$. These walls will be rough with a transverse width $W$ on a scale $\ell$ described by the roughness exponent $\zeta$, $W \sim \ell^\zeta$. But at the critical point, we expect the walls will become fractal. The definition of a domain wall in the RFIM has ambiguities because some isolated clusters of spins — in particular those with anomalously strong random fields — are *frozen*, i.e., unaffected by changes in boundary conditions. The identification of the bonds that define the domain wall is therefore uncertain up to these fixed spins. We use three methods for calculating the fractal dimension of the domain walls introduced by changes in the boundary conditions; each definition has a distinct physical import in a scaling picture of the RFIM.

One method is to determine the surface area of the set of spins connected to one face of the sample that are *unchanged* when the spins on the *opposite face* are reversed. This yields a *spanning surface* of a dimension that we denote $d_s$. The second method is based on a box counting approach that counts which volumes in a system with antiparallel boundary conditions differ from *both* the "up" and the "down" configurations obtained from parallel spin boundary conditions; this we denote $d_I$, to indicate its role as a measure of the volume locally incongruent with these two configurations.

A third method does not measure a dimension directly but rather an energy: the contribution of the exchange interactions to the stiffness at the critical point. As will

be explained later, this fractal dimension, $d_J$, is *not* expected to be an independent exponent. Rather, it is related to the others by

$$d_J = \theta + 1/\nu, \qquad (9)$$

a relation obtained by considering the derivative of the stiffness with respect to $h$. It can be seen that our results for the exponents are entirely consistent with this scaling law.

The three exponents associated with the fractal dimension of the critical domain walls are similar, but perhaps not all mutually consistent, given the estimated error bars:

$$d_s = 2.30 \pm 0.04 \qquad (10)$$
$$d_I = 2.24 \pm 0.03 \qquad (11)$$
$$d_J = 2.18 \pm 0.03 \qquad (12)$$

As we will discuss, we believe that at least two of these dimensions indeed measure slightly distinct quantities, due to frozen spin clusters that are relatively independent of boundary conditions. The simplest plausible conjecture is that $d_J = d_I < d_s$, though it may be that $d_J$ and $d_I$ are distinct.

### C. Magnetization

As mentioned above, some previous studies have found that the magnetization appears to be discontinuous at the transition. Indeed, our data for the magnetization as a function of size for various types of boundary conditions that were chosen so that some favor a ferromagnetic state while others favor a disordered state, *appear* to be consistent with the coexistence of three states at the critical point as was found in other recent work.[13] But, as discussed below, we believe that this conclusion is influenced by the nearness of $\beta/\nu$ to zero. Based upon the scaling picture and numerical evidence, we will argue that, at the critical point there is only a single state and the apparent "up" and "down" configurations do *not* correspond to distinct states in the infinite volume limit.

Using the magnetization data and the best fit critical point found from our studies of the stiffness, we can attempt to extract an estimate for the scaling of the magnetization with system size at the critical point. This yields

$$\frac{\beta}{\nu} = 0.012 \pm 0.004 \qquad \text{[magnetization]}, \qquad (13)$$

which is *inconsistent with zero* at the level of three standard deviations. The primary uncertainty in our estimate of $\beta/\nu$ arises from the uncertainty in the value of $h_c$, as the statistical errors in the sample average $\overline{|m|}$ are relatively small at fixed $h$. This exponent describes the magnetization very well for systems of size $32 \leq L \leq 256$, for a range of $h_c$, $2.265 < h_c < 2.275$.

## D.  Spin clusters and walls

In spite of the smallness of $\beta$, useful information on the decay of spin correlations at the critical point can be obtained indirectly by studying the statistical properties of the domain walls separating connected clusters of parallel spins. In the ferromagnetic phase, we expect that the probability of finding a region of diameter $\ell$ that is not affected by the boundary conditions decays exponentially for $\ell \gg \xi$ as $\exp(-C(\ell/\xi)^{d-2})$.

Since the system *appears* to be ferromagnetic at the critical point, due to $|m|$ being nearly unity for the system sizes studied, we also study clusters of the minority spins at $h \approx h_c$. The clusters are defined hierarchically starting from the largest connected cluster of connected spins, with the surface of each cluster given by its *outermost* surface, that is, the set of bonds connecting it to the surrounding cluster. The volume of each cluster *includes* that of the fully enclosed subclusters of the opposite sign (and their subclusters, if any, etc). But the outer surface of a cluster does *not* include the *surfaces* of its fully enclosed subclusters, whose number scales with the volume of the cluster.

The outer cluster surfaces are found to be fractal with mean area $\overline{a}$ (averaged over clusters and samples) scaling with enclosed volume $v$ as

$$\overline{a}(v) \sim v^{d_s^c/d} \tag{14}$$

with the exponent

$$\frac{d_s^c}{d} \simeq 0.755 \pm 0.008, \tag{15}$$

suggesting a surface fractal dimension $d_s^c \simeq 2.26 \pm 0.02$, a value consistent with the domain wall dimension $d_s$.

Perhaps more interesting is the distribution of the *number density* of spin clusters as a function of their size, in particular the probability $\rho(v)$ that a given site is in a minority spin cluster of size of order $v$ — more precisely,

$$\rho(v) \equiv \frac{v}{\delta v}\text{Prob}[\text{site} \in \text{cluster of size in } (v, v+\delta v)]. \tag{16}$$

We find that over the range of sizes studied $\rho(v)$ appears to converge to a *small constant* value, $\rho_\infty$, for $1 \ll v \ll L^3$, with periodic boundary conditions. This implies that in the limit of an extremely large system, any given spin will definitely be in such a "minority spin" cluster; indeed, it will typically be within one such large cluster which itself will be within a cluster of typical size $\sim \rho_\infty^{-1}$ larger which itself will be in an even larger cluster, etc. This is exactly the type of behavior that gives rise to power law decay of spin correlations at a critical point on sufficiently long scales, as is explained in Section IX. It is consistent with expectations from other observations we have made, in particular that the probability that the stiffness of a finite sample is exactly zero tends to a non-zero constant for large system sizes at the critical point.

The value of

$$\rho_\infty \simeq 0.0019 \pm 0.0004 \tag{17}$$

that we find[28] yields an estimate for

$$\beta/\nu = 2d\rho_\infty \simeq 0.011 \pm 0.003 \qquad [\text{cluster}] \tag{18}$$

consistent with Eq. (13). This exponent controls the decay of the typical magnetization with system size at the critical point:

$$m(h_c) \sim L^{-\beta/\nu}. \tag{19}$$

For $L = 128$, this only gives a reduction factor of 0.94 from the magnetization of a small system and is consistent with our magnetization data. Note that with this estimate, one would need to go to system sizes of order $10^{21} \lesssim L \lesssim 10^{38}$ to see a factor of two reduction in the magnetization at the critical point!

For the magnetization in the ferromagnetic phase, using this calculation of $\beta/\nu$ and consistent with the finite size scaling of the magnetization, we expect conventional behavior with

$$m \sim (h_c - h)^\beta \tag{20}$$

but with

$$\beta \simeq 0.017 \pm 0.005 \tag{21}$$

— far smaller than for any other known system with the exception of the one-dimensional Ising model with long-range $1/r^2$ interactions which has a critical transition with a discontinuous magnetization, i.e. $\beta = 0$.[29] This small value is near the value $\beta = 0.02$ suggested from numerical renormalization group calculations on a hierarchical lattice.[30] The numerical value we find is consistent with several previous studies: for example, Hartmann and Nowak determine $\beta = 0.02 \pm 0.01$, using exact ground states[11], Swift, *et al*,[10] find $\beta = 0.025 \pm 0.015$, and Rieger[12] found $\beta \approx 0$ at positive temperature, but without any latent heat or multipeak structure in the magnetization distribution, suggesting a second order transition. However, we can more clearly exclude $\beta/\nu = 0$ as a possibility by making use of connections between the value of $\beta/\nu$ and the statistics of spin clusters.

One question that naturally arises concerns the structure of spin clusters for small $|m|$ near the critical point, where the sample no longer *appears* ferromagnetic. Is there a possibility of percolation of both up and down spins, when $|h - h_c| \lesssim 10^{-(22\pm8)}$ in large enough samples? For fixed $+$ or $-$ boundaries, as $h \to h_c$, $|m|$ becomes small, but the minority and majority spins are not independent. Hence, even though the density of $+$ and $-$ spins becomes almost equal, the minority spins are large clusters embedded within the matrix of majority spins, so that *only one sign of spin percolates in the disordered phase* even close enough to the critical point that the magnetization is very small and the density of minority

spins almost one half. Exactly at the critical point in an infinite sample, or where $\xi > L$ in a large finite sample, the long length scale characterization of the spin configuration will be rather different than in either phase; these differences motivated some aspects of the present numerical study.

### E. Number of states

To study the RFIM phases and transition in more detail, we have analyzed the influence of boundary conditions on a window of size $w$ in the center of a sample as the sample size $L$ diverges. As made clear by Newman and Stein[31], the character of the thermodynamic limit of the ground states can be investigated by studying such windows. Our numerical computations strongly support the picture of a small number of ground states — two in the ordered phase and one in the disordered phase — consistent with the simple scaling scenario.[21,32]

Nevertheless, because $\beta/\nu$ is so small, at the critical point it it is difficult to use numerics to directly distinguish between two scenarios: (A) two coexisting states, as in the ferromagnetic phase; or (B) a single state, with interior spins unaffected by boundary conditions as $L \to \infty$. If $\beta$ were exactly zero, as in (A), then the probability $q$ that boundary conditions could affect spins in the center in ways other than the apparent "up" and "down" phases would decay as a power of the system size,[22,23] $q \sim L^{d_s - d}$, where $d_s$ is the fractal dimension of domain walls. In scenario (B), a similar power law scaling is expected, with $q \sim L^{d_s - \beta/\nu - d}$, where the change in exponent reflects the freezing of spins or, equivalently, decay of magnetization, as $L \to \infty$. As will be argued below, the simplest expectation is that the exponent $d_I = d_s - \beta/\nu$, so that $q \sim L^{d_I - d}$. This is consistent with the assumption of only one state at criticality.

### IV. OUTLINE

The remainder of the paper gives the details of the numerical results and related scaling arguments. Table I is a summary of the numerical values of the exponents. In Sec. V, we describe how the stiffness is computed and demonstrate that its scaling is quite consistent with a "conventional" second order phase transition. To aid in developing understanding, we study how the probability that the stiffness is exactly zero depends on the sample shape. Sec. VI presents the three methods that we employ to compute the dimension of the domain walls generated by comparing different boundary conditions (the same comparison used when calculating the stiffness.) The methods differ somewhat in how they count regions of "frozen" spins that are not affected by boundary conditions. In the subsequent section (Sec. VII), we report results on the magnetization $m$ near $h_c$. Though the distribution of $m$ depends strongly on boundary conditions,

the scaling of these distributions are quite consistent with a single value of $h_c$ (and also consistent with the methods of finding $h_c$ in other sections.) Our study of the scaling of the surfaces of spin clusters with their volumes is summarized in Sec. VIII. Besides giving a fractal dimension $d_s^c$ consistent with the domain wall dimension $d_s$, these computations can be used to separately infer $\beta/\nu$, given an understanding of magnetization and correlation functions based upon a domain wall picture. Our estimates for the singular behavior of the specific heat are included in this section. The general scaling picture that connects these results is reviewed in more detail in Sec. IX. In Sec. X, we report results of how the spin configurations depend on sample size and boundary conditions for a fixed disorder realization. These results are consistent with a single transition separating a (large $h$, disordered) phase with a single thermodynamic limit from a (small $h$, ordered) phase with two distinct thermodynamic limits. In the Summary (Sec. XI), we review the scenario for the transition that is consistent with the numerical results and contrast this scenario with alternate pictures.

### V. STIFFNESS AND SCALING

To establish the location and nature of the transition, we first focus on the stiffness of the system. In an ordered Ising phase, the (free) energy of a domain wall across a system of size $L^d$ will be $\Sigma \approx \sigma L^{d-1}$ with $\sigma$ the interfacial tension. At an ordinary first order transition, the interfacial tension is discontinuous at the transition, while near a second order transition, it goes smoothly to zero. For a zero-temperature transition, the interfacial tension vanishes with a variant of Widom scaling[2]

$$\sigma \sim (h_c - h)^{(d-1-\theta)\nu}. \tag{22}$$

To probe the stiffness of a random system takes some care. For a random field system, there is no exact symmetry between the up and the down spins but only a *statistical symmetry of the distribution* of the random fields. Thus, for example, for a given sample in the ordered phase, the energy of the up state — obtained with up boundary conditions (BCs) — will differ from that of the down state (obtained from down BCs), by a random amount of order $\sqrt{\mathcal{V}}$ arising from the differing effects of the random fields on the two states. In order to compute the interfacial energy it is useful to subtract as much as possible of this random "bulk" energy so as to be left with a quantity that is as-close-as-possible to an "interfacial" energy.

#### A. Definition of the stiffness

To obtain the stiffness of a sample, we compute the *symmetrized energy difference* between antiparallel and parallel boundary conditions. This is computed from the

TABLE I: Table of numerical estimates. The exponent or constant name, computed value, primary method for inferring the value, section discussed, and most relevant figure are listed.

| Symbol | Value | Definition and data used |
|---|---|---|
| $\theta$ | $1.49 \pm 0.03$ | Scaling of stiffness at $h_c$, violation of hyperscaling. |
| | | Found from scaling of stiffness with $L$ and $h - h_c$, see Sec. V and Fig. 2. |
| $h_c$ | $2.270 \pm 0.004$ | Critical value of the random field. |
| | | Determined from constancy in $P_0$, probability of zero stiffness (see Fig. 4 and Sec. V), |
| | | and consistent with estimates from convergence of effective dimension estimates $\tilde{d}_{s,I,J}$, |
| | | scaling of $\Delta_{m^2}$ peak locations with $L$, scaling of $|m|$ with $L$ (Fig. 19), |
| | | and window change probabilities (Fig. 29). |
| $\nu$ | $1.37 \pm 0.09$ | Correlation length exponent. |
| | | Found from scaling of the stiffness with $L$ Sec. V and Fig. 2, with $h_c$ fixed by $P_0$ measurements. |
| | | Consistent with scaling of $\Delta_{m^2}$ peak locations with $L$. |
| $\zeta$ | $0.66 \pm 0.03$ | Roughness of domain walls in the ferromagnetic phase. |
| | | Found using anisotropic scaling (Fig. 13) and effective exponent in $L^{2/3} \times L^2$ samples. |
| | | See Sec. VI C. |
| $d_s$ | $2.30 \pm 0.04$ | Fractal dimension of connected domain wall at $h = h_c$. |
| | | Found from surface of $\mathcal{U}_{++,+-}$, as shown in Fig. 11. |
| | | See Fig. 12 and Sec. VI B. |
| $d_I$ | $2.24 \pm 0.03$ | "Incongruent" fractal dimension of domain wall at criticality. |
| | | Box counting of incongruent volumes (disconnected wall). See Fig. 15 and Sec. VI D. |
| | | Consistent with scaling of state overlap probabilities shown in Fig. 29. |
| $d_J$ | $2.18 \pm 0.03$ | Energy "fractal dimension" at $h = h_c$. |
| | | Found from the exchange part, $\Sigma_J$, of the stiffness. |
| | | See Fig. 16 and Sec. VI E. |
| $d_s^c$ | $2.27 \pm 0.02$ | Fractal dimension of the surface of spin clusters. |
| | | See Fig. 22 and Sec. VIII A. |
| $\rho_\infty$ | $0.0019 \pm 0.0004$ | Probability per scale $e$ of crossing a spin cluster surface at $h = h_c$. |
| | | See Sec. VIII B and Figs. 23, 23, and 25. |
| $\beta/\nu$ | $0.011 \pm 0.003$ | Ratio of magnetization exponent to $\nu$. |
| | | Determined from $\rho_\infty$ and consistent with scaling of $|m|$ vs. $L$ at criticality. |
| | | See Fig. 19 and Sec. IX A. |
| $\beta$ | $0.017 \pm 0.005$ | Magnetization exponent, found from $\beta/\nu$ and $\nu$. |
| $(\alpha - 1)/\nu$ | $-0.74 \pm 0.02$ | Combination of heat capacity exponent $\alpha$ and $\nu$ |
| | | Found using value for $d_s^c$ and Eq. (56). |
| $\alpha$ | $-0.01 \pm 0.09$ | Heat capacity exponent, found using Eq. (56) and $\nu$. |
| | | Consistent with modified hyperscaling Eq. (6) and the value $\alpha = -0.12 \pm 0.12$ found |
| | | from a fit to the bond energy density $E_J(L)$ at $h_c$ and $\nu$. |

ground state energies for four different boundary conditions on a given sample, denoted $++$, $+-$, $-+$ and $--$. These correspond to fixing the spins to have values $s = +1$ or $s = -1$ on the left or right sides while imposing periodic boundary conditions in the other two directions. For example, $+-$ has spins fixed to $+1$ on the left and to $-1$ on the right. The interface energy is then defined as[32]

$$\Sigma \equiv (E_{+-} + E_{-+} - E_{++} - E_{--})/2. \qquad (23)$$

Note that the average over samples of $\Sigma$ will be the same as that of $E_{+W} \equiv E_{+-} - E_{++}$. Studying $\Sigma$, however, reduces the effects of energy changes near the boundaries

that are caused by the differing boundary conditions: in $\Sigma$, each boundary condition on each side appears twice but with opposite signs so that these effects cancel. This cancellation will be most pronounced well into the disordered phase.

In the *disordered phase*, the boundary conditions typically only affect layers near the boundaries with thickness of order the correlation length $\xi$; deep in the interior (for system sizes $L \gg \xi$) the spins will be frozen, completely unaffected by the boundary conditions. The *average* energy of the boundary layers will, because of the statistical symmetry, be independent of whether the boundary conditions are plus or minus. But there will

be a random part of the boundary energy, with magnitude of order $\sqrt{L^{d-1}}$, that *is* sensitive to the boundary condition. Thus in three dimensions, $E_{+W}$ will typically be of order $L$ even in the disordered phase. In contrast, the stiffness $\Sigma$ will typically be exactly zero because of the cancellation of the boundary energies and the concomitant frozen interior which blocks any knowledge of the spins near one face about the boundary conditions on the opposite face. In general, the distribution for $\Sigma$ contains a $\delta$-function contribution with some weight

$$P_0 \equiv \text{Prob}[\Sigma = 0]. \qquad (24)$$

Sample configurations from simulations are illustrated in Fig. 1 with two-dimensional slices shown. Part (a) of the figure illustrates a situation somewhat into the disordered phase in which the left and right boundaries are effectively decoupled as discussed above. The *frozen spins*, those that are the same with all four boundary conditions, are indicated by dark or white squares in part (c) of the figure, while those that are affected by the BCs, the controllable spins, are indicated by gray squares.

The behavior in the *ordered phase* is quite different as can be seen in the parts (b) and (d) of Fig. 1. In this case, the difference between the $--$, the $+-$ and the $++$ boundary conditions can be well characterized by a $+|-$ domain wall that has a minimum energy position somewhat to the left of the center. Similarly the difference between the $--$, the $-+$ and the $++$ boundary conditions is characterized by a $-|+$ domain wall whose minimum energy position is somewhat to the right of the center. The stiffness of this sample will thus be half the sum of energies of the two types of walls *plus* the energy of the random fields (here predominantly negative) in the region between the two favored positions of the walls; the contribution of the random fields in this region will *not* cancel.

This picture yields a stiffness in the *ordered phase* with a mean of order $L^{d-1} = L^2$ and variations around this mean of order $L^{d/2} = L^{\frac{3}{2}}$, the variations being dominated by the random fields in between the positions of the two types of walls. In the ordered phase for $h < h_c$, $P_0 \to 0$ — apparently exponentially fast or faster in $L$ — as $L \to \infty$.

At the *critical point*, the behavior is qualitatively like that in the ordered phase. But here the energy cost of the interface is much lower, the interface itself is fractal, and, in the regions of controllable spins that are otherwise flipped by the changing boundary conditions, there are large frozen unflipped "holes".

## B. Statistics of the stiffness

The stiffness $\Sigma$ was determined by finding the ground states for a single sample subject to each of the four boundary conditions $++$, $--$, $-+$ and $+-$. By studying many samples, we computed the distribution of $\Sigma$ for various system sizes and random field strengths. In particular, we computed both the probability $P_0$ that $\Sigma = 0$
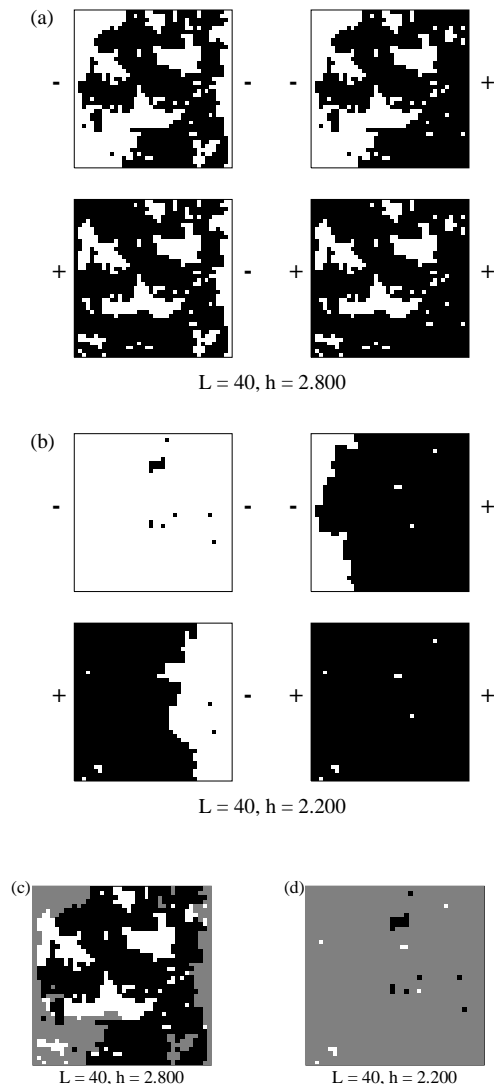


FIG. 1: Pictures of planar slices ($z = 0$ ) of configurations, for fields (a) $h = 2.8$ and (b) $h = 2.2$, in samples of size $40^3$. The slices shown at each $h$ are the four combinations of boundary conditions $--$ (top left), $-+$ (top right), $+-$ (bottom left), and $++$ (bottom right), where the left and right faces (in the $x$ direction) are fixed $+$ or $-$ and periodic boundary conditions are in effect for the $y$ (up/down) and $z$ (out of the page) directions. The dark squares indicate an up spin at that location in the slice. The $--$ and $++$ visualizations for $h = 2.2$ show the presence of minority spin "bubbles" embedded in the bulk. A summary of the effect of the boundary conditions for $h = 2.8$ and $h = 2.2$ are shown in parts (c) and (d), respectively. Dark and light squares correspond to up and down spins, respectively, that are *frozen*, i.e., invariant under this set of boundary conditions. The gray *controllable* spins can be modified by choosing among the four boundary conditions. For $h = 2.8$, the gray volume is composed of two unconnected regions anchored on the two controlled boundaries, so that the stiffness $\Sigma = 0$. In contrast, at $h = 2.2$, in the sample shown, the gray region connects the two sides and $\Sigma \neq 0$.

as well as the mean stiffness $\overline{\Sigma}$, denoting, as usual, averages over the randomness by overlines. For the bulk of the computations, ground states were found for cubic samples of size $L^3$ and anisotropic samples of size $2L \times L^2$ with the length along a (100) axis of the lattice perpendicular to the controlled faces, the $x$-direction, being $2L$. To check that the results were not artificially influenced by lattice orientation effects, we also computed values of $\Sigma$ for two types of samples whose controlled faces are $L \times L$ rhombi, with $L$ and $4L$ layers, respectively, separating the two faces along the (111) direction. Note that such (111) layers are separated by a distance of $1/\sqrt{3}$, rather than the distance of 1 that separates the (100) layers. As the lattice in both of these geometries is cubic and the ferromagnetic couplings are the same, the $h_c$ found should be the same in the two orientations.

If the transition is second order, the mean interface energy should scale as

$$\overline{\Sigma} \approx \overline{C} L^{\theta} \mathcal{S}[L^{1/\nu}(h - h_c)K], \tag{25}$$

where the exponent $\theta$ sets the scaling of the energy at the critical point, $\nu$ is the correlation length exponent, $\mathcal{S}$ a universal scaling function that depends on the *shape* of the sample, and $K$ and $\overline{C}$ are non-universal coefficients. Using this scaling form and varying $\theta$, $\nu$ and $h_c$ yields a good collapse of the data, as shown in Fig. 2 for the (100) samples. By varying the exponents in the scaling plot, we estimate the values $h_c = 2.27 \pm 0.01$, $\theta = 1.50 \pm 0.08$ and $\nu = 1.35 \pm 0.20$. Using the data for $P_0$ to fix $h_c = 2.270$ as discussed below, gives $\theta = 1.49 \pm 0.02$ and $\nu = 1.37 \pm 0.09$. The excellent collapse of the data strongly support the conclusion that the phase transition is second order.

The value of $\theta$ is in quantitative agreement with results from Monte Carlo simulations at finite temperature,[12] which found $\theta = 1.53 \pm 0.10$. It is also within the bounds determined from various arguments:

$$\frac{d}{2} - \frac{\beta}{\nu} \leq \theta \leq \frac{d}{2}; \tag{26}$$

the lower bound arising from scaling laws and a rigorous inequality[2,33]. The upper bound follows from the observation that any larger value of $\theta$ would imply that the system would be stable — by the argument of Imry and Ma[34] — to an increase of the random field and thus should not be at the critical point. Since $\beta/\nu$ is extremely small, we expect that the true value of $\theta$ should be just slightly below $3/2$. This is to be contrasted with the "dimensional reduction" result predicted to obtain to all orders in a $d = 6 - \epsilon$ expansion of $\theta = 2$ (but see recent claims in Ref. 35).

The correlation exponent $\nu$ must be no smaller than $2/d$ in random systems.[36] Our result easily satisfies this bound. Indeed, it is substantially larger than this lower bound and even more so than the mean-field value of one half; this is presumably associated with proximity to the lower critical dimension of $d_\ell = 2$.
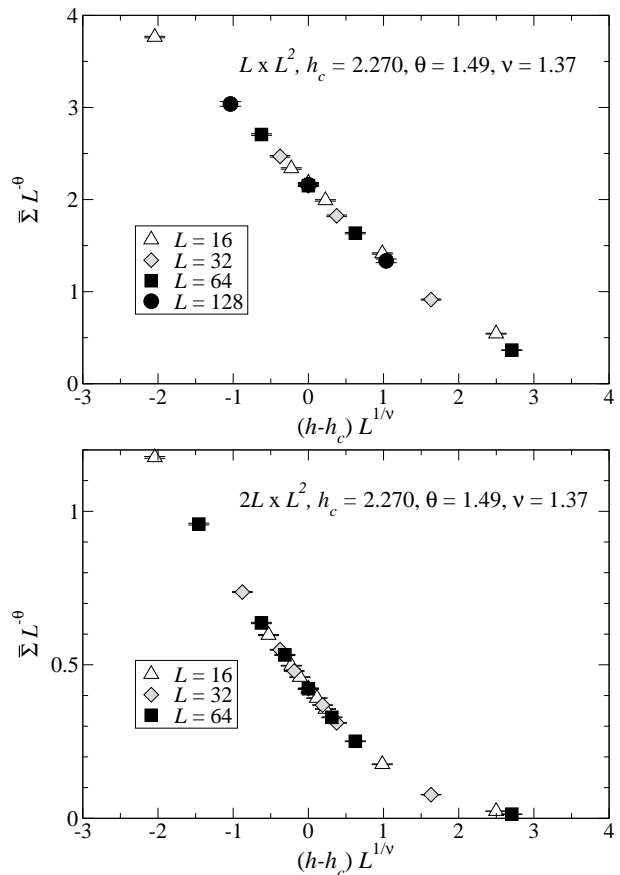


FIG. 2: Scaling plot for the sample averaged stiffness $\overline{\Sigma}$ for (a) isotropic samples of volume $L^3$ and (b) anisotropic samples of volume $2L \times L^2$, with the longest axis being the direction in which the boundary conditions are varied. Note that the vertical scales differ. The stiffness is calculated by the symmetric comparison of four ground state energies: the energies for the four choices of spin up and spin down boundary conditions on the left and right sides and with periodic boundary conditions in the other two directions. The fit shown is for energy exponent $\theta = 1.49$, correlation length exponent $\nu = 1.37$ and critical value $h_c = 2.270$. This scaling is consistent within errors, except for the $L = 16$ isotropic samples. Statistical ($1\sigma$) error bars are shown.

### 1. Stiffness in the disordered phase

Fig. 3 shows the dependence of the mean stiffness on the linear dimension $L$ for the $L \times L^2$ samples. The decay of the stiffness is well fit by a decaying exponential $\overline{\Sigma} \sim \exp(-L/\xi_\Sigma)$, for $h > h_c$ and $L \gg \xi_\Sigma$ (roughly when $\overline{\Sigma} < 0.2$.) The correlation length can be inferred from the fits. The values for $\xi_\Sigma$ obtained from the $2L \times L^2$ samples, using a similar plot, are in agreement with those from the cubic sample to within 10% for each $h$. The values of the correlation lengths $\xi_\Sigma$ found are consistent with a divergence of $\xi_\Sigma \sim (h - h_c)^{-1.3 \pm 0.1}$, taking $h_c = 2.27$, consistent with our other determinations of $\nu$, though the data is not very near $h_c$. It may be possible to make a
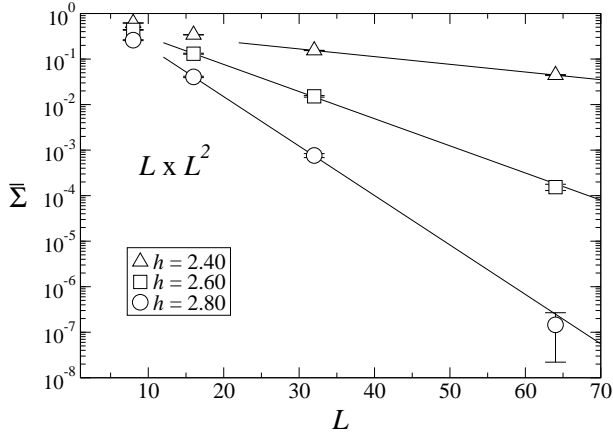
FIG. 3: Plot of the decay of the mean stiffness $\overline{\Sigma}$ with $L$, in the disordered phase. The lines are fits to the data for $\overline{\Sigma} < 0.2$ of the form $\overline{\Sigma} \sim \exp(-L/\xi_\Sigma)$. In conjunction with similar fits for $2L \times L$ samples, which allow us to estimate errors from finite size fitting, we find the values $\xi_\Sigma = 26 \pm 4$, $7 \pm 1$ and $4.0 \pm 0.4$ for $h = 2.4$, 2.6, and 2.8, respectively.

more accurate determination of $\nu$ by more careful calculations using $h$ values somewhat nearer to $h_c$.

For the $2L \times L^2$ samples, $P_0$, the probability of the stiffness being zero, can be appreciable for accessible $L$ and $h$ near $h_c$. The data for fixed $h \geq h_c$ are consistent with $P_0$ approaching one exponentially with $L$, although other forms cannot be ruled out.

### 2. Stiffness at criticality

At the critical point, a non-trivial scaling function

$$P_c(\Sigma/CL^\theta) \equiv P(\Sigma/CL^\theta, 0) \qquad (27)$$

for the distribution of $\Sigma$, would suggest that $P_0$ should approach a *finite fixed point value*. In Fig. 4(a) a plot of $P_0$ is shown as a function of $L$ for various $h$. Observe that opposite boundaries are almost always coupled at $h_c$ in the cubic samples:

$$P_0^{\mathrm{cubic}}(h_c) \simeq 0.04 \pm 0.01 \qquad (28)$$

This value for $P_0$ is so small that to verify that $P_0$ indeed approaches a non-zero constant at the transition, we also performed simulations for anisotropic samples of various shapes. In general, we expect that the distribution of $\Sigma$ at the critical point, $P_c$, will depend on the *shape* of the sample with long thin samples typically yielding lower stiffness and a higher probability of the stiffness vanishing than short fat ones of the same cross section.

For rectilinear samples of dimensions $2L \times L^2$, with the controlled boundaries at opposite ends of the *long* (100) axis, we find that $P_0$ approaches a value well away from zero, $P_0 = 0.298 \pm 0.005$, at $h = 2.270$ (Fig. 4(b)). For rhomboidal samples with $L^3$ spins consisting of $L$ layers and a length along the (111) control axis of $L/\sqrt{3}$,
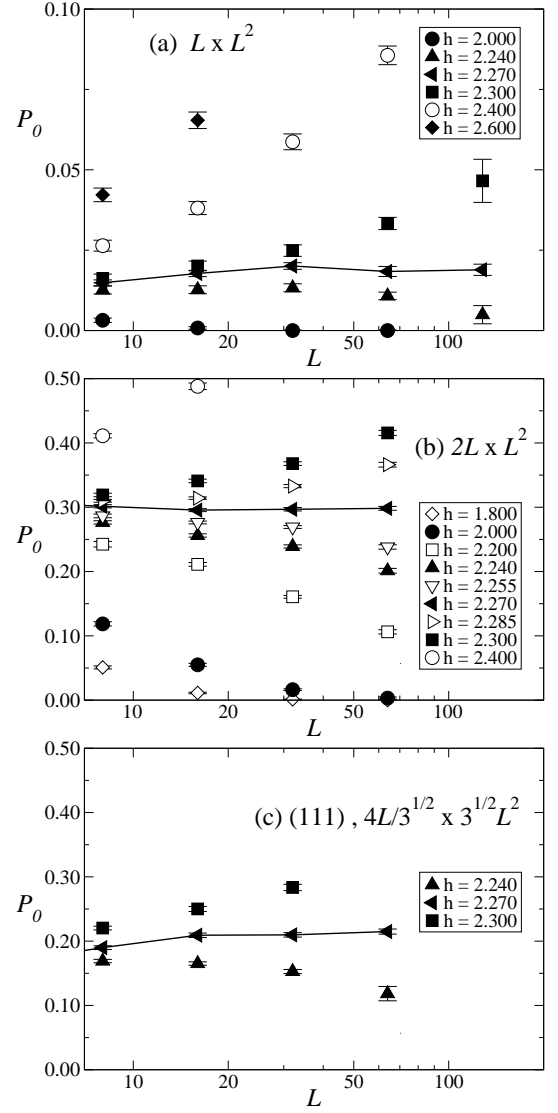


FIG. 4: Plot of the probability $P_0(h, L)$ that the stiffness $\Sigma$ is zero, for (a) isotropic samples of volume $L^3$ and (b) anisotropic samples of volume $2L \times L^2$, with the longest axis being the direction in which the boundary conditions are varied, and (c) anisotropic samples of volume $4L^3$, with the boundary faces in the (111) plane. For all sample shapes, the convergence to a fixed value of $P_0$ as $L \to \infty$ for $h = 2.270$ suggests the location of the critical point. The solid lines connect the points for $h = 2.270$ to demonstrate convergence of $P_0$ to a constant, within statistical errors. As $P_0$ is very nearly zero for isotropic samples ($P_0(2.27, \infty) \approx 0.04$, if the apparent convergence holds at large $L$), the errors in determining $h_c$ are larger. From the $2L \times L^2$ anisotropic samples, where the apparent extrapolation is $P_0(2.27, \infty) = 0.298 \pm 0.05$, $h_c = 2.270 \pm 0.004$. For the (111) oriented samples, with volume of $4L/\sqrt{3} \times \sqrt{3}L^2$ (layer separation $\times$ layer area), the data is also consistent with $h_c = 2.270$, with $P_0 = 0.23 \pm 0.01$. Separate results, not shown, for (100) samples of shape $4L \times L^2$ give a value of $P_0(2.27, 16 \leq L \leq 64) = 0.79 \pm 0.02$.
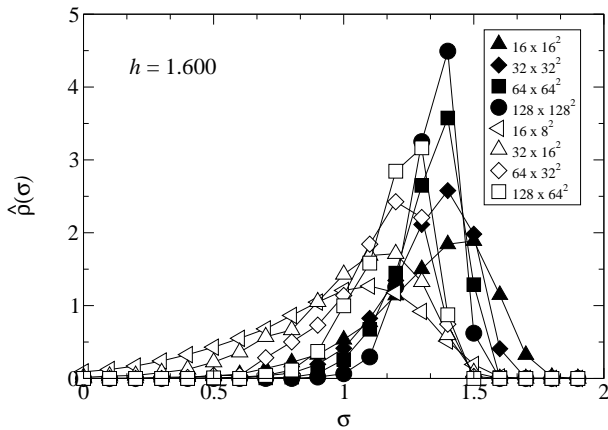
FIG. 5: Probability density $\hat{\rho}(\sigma)$ of the values of the interfacial energy density $\sigma = L^{-2}\Sigma$ in the ordered phase with $h = 1.60 < h_c$. As the sample size grows larger, the relative sample-to-sample variations of $\sigma$ decrease, consistent with an approach to a $\delta$-function at the mean value $\sigma(h = 1.6) \approx 0.69$, for both the $L^3$ and $2L \times L^2$ samples,
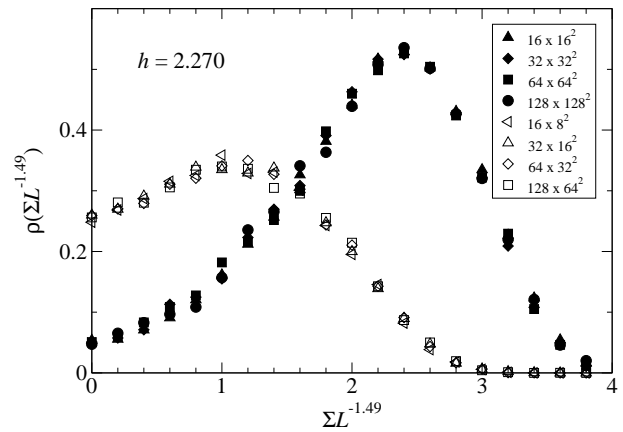


FIG. 6: Probability density $\rho(\Sigma)$ of the scaled non-zero values of $\Sigma L^{-\theta}$ with $\theta = 1.49$, for $h = 2.270 \approx h_c$. A $\delta$-function at $\Sigma = 0$ with weight $P_0 \approx 0.04$ ($\approx 0.298$) for the $L^3$ ($2L \times L^2$) samples is not shown. The distributions for samples with linear dimensions $L$ greater than 16 are statistically consistent with a fixed point distribution for $\Sigma$, with a characteristic scale $\Sigma_0 \sim L^{1.49}$ and a form dependent on the shape of the samples.

$P_0$ is not distinguishable from zero. However, for longer rhomboidal samples with $4L^3$ spins consisting of $4L$ layers and a length $4L/\sqrt{3}$ along the control axis, we find $P_0 = 0.21 \pm 0.01$ at $h = 2.270$ for $16 \leq L \leq 64$ (Fig. 4(c)). Imposing convergence of $P_0$ to a fixed (non-trivial) value as $L \to \infty$ gives a critical value of $h_c = 2.270$. These anisotropic rectilinear and long rhomboidal samples yield our most precise estimate for $h_c$, Eq.(3).

We should expect $P_0$ to be a smooth function of the shape; the fact that it is far from zero in samples with aspect ratio of order two lends strong support to the conjecture that it will be non-zero for any shape. The observation that it is small for cubical samples is related, as will be explained below, to the smallness of $\beta$.

### 3. Comparison of distributions for $\Sigma$

The complete probability distributions for $\Sigma$ at various values of $h$ are plotted in Figs. 5 through Fig. 8 for both the cubical and the elongated (100) samples. For $h = 1.6$, the distribution of $\Sigma$ appears to approach a narrow distribution about $\Sigma \approx (1.39)L^2$, regardless of sample shape; this is as expected for the ordered phase. For $h = 2.27$, the critical point, the distribution obeys the simple scaling form of Eq.(2) for both the isotropic and anisotropic samples but with a different scaling functions for each of the two shapes. Fig. 8 shows the integrated probability distributions for $h = 2.40$. As $L$ increases, the mean interfacial energy decreases approximately exponentially, and $P_0$ approaches 1.
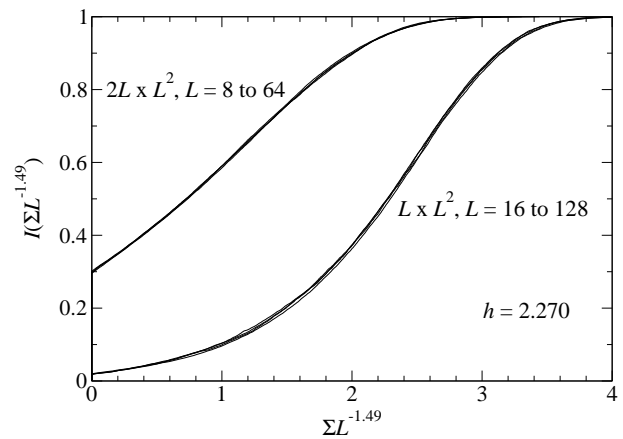


FIG. 7: Scaling plot for the cumulative distribution $I(\Sigma) = \int_0^{\Sigma} d\Sigma' \rho(\Sigma')$ of the stiffness, for $h = 2.270 \approx h_c$. The stiffness $\Sigma$ has been scaled by the energy scale $L^{\theta}$, with $\theta = 1.49$. The labels indicate the sample shapes ($2L \times L^2$ and $L \times L^2$) for each set of curves. For each sample shape, four sample sizes are plotted ($16 \times 8^2 \to 128 \times 64^2$ and $16^3 \to 128^3$.) At the resolution shown, the scaled curves are nearly independent of $L$. The intercept at $\Sigma = 0$ corresponds to $I(0) = P_0$, the probability of a sample having zero stiffness. As in Fig. 6, the curves converge to a fixed point distribution.

## VI. GEOMETRY OF DOMAIN WALLS

In addition to the scaling properties of the energies of domain walls, we are also interested in their geometrical properties. These properties are expected to be related to the properties of the surfaces of spin clusters that are either frozen or induced by bulk perturbations (as opposed to boundary perturbations), to the effects of boundary
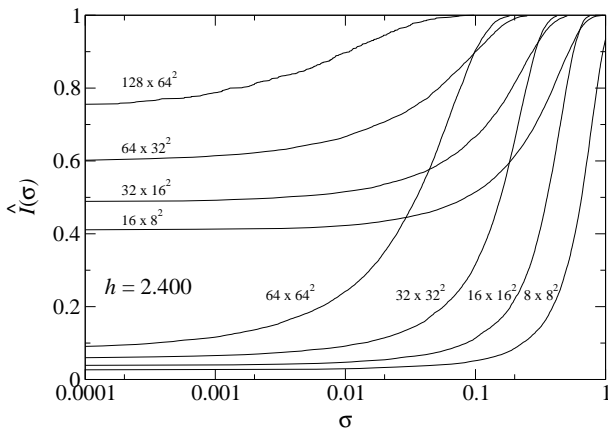
FIG. 8: Cumulative distribution $\hat{I}(\sigma) = \int_0^\sigma d\sigma' \hat{\rho}(\sigma')$ for $h = 2.400 > h_c$. As the sample size increases, $P_0$, given by the intercept of the curves at $\Sigma = 0$, increases, and the typical non-zero values of $\sigma \equiv \Sigma L^{-2}$ rapidly decrease. From Fig. 3, the length scale for the decay of the stiffness is $\xi_\Sigma = 26 \pm 4$. This length is comparable to the mid-range system sizes here. Note that $P_0$ rises more quickly and the typical non-zero $\sigma$ decays more rapidly with $L$ in the anisotropic samples.

conditions on the deep interior of a sample, and to the general scaling picture for the transition.

In the ferromagnetic phase, the interfacial tension $\sigma$ is positive. The domain walls will appear flatter and flatter on large length scales with surface area proportional to $L^2$ but nevertheless divergent roughness characterized by a roughness exponent $\zeta = 2/3$ and random energy variations that scale as $L^{\theta_I}$, with $\theta_I = 4/3$.[37,38,39,40]

At the critical point, the interfacial tension of the walls vanishes. Thus we should not except them to be flat even on large scales; the natural expectation is that they will be fractal with surface area scaling as

$$A \sim L^{d_s} \tag{29}$$

with $d_s$ a *fractal dimension*. One might expect, *a priori*, that the exponent $d_s$ would be an independent exponent as it is not obviously related to $\theta$, $\beta$, and $\nu$. For the simple scaling scenario to obtain, we expect $d_s$ to be in the range:

$$d - 1 < d_s < d. \tag{30}$$

If the transition were first order, one would expect $d_s = d - 1$ as in the ferromagnetic phase (more precisely, some fraction of samples at the transition would show such interfaces). If, at the other extreme, it were found that $d_s = d$, this would mean that the "walls" would be space-filling (up to possible logarithmic factors); this would cast doubt on the overall scaling scenario for excitations, etc, near the phase transition.[2]

## A. Frozen spin regions

To study interfaces we would like to compare the spin configurations found using the boundary conditions $++$, $+-$, $-+$, and $--$ as discussed in the previous section. But in random field systems, there is an intrinsic difficulty associated with defining an interface: this arises from the presence of frozen regions which are not affected by changing from $++$ boundary conditions to $--$ boundary conditions and thus are unaffected by *any* changes in the boundary conditions on the controlled surfaces.[41] With mixed boundary conditions, say $+-$, the interface between the region that is like the "up" ($++$) state and the region that is like the "down" ($--$) state can pass along the boundary of the frozen regions. Are we to count such sections as truly part of the interface? Or should we exclude the frozen regions from the system and think of the interface as bisecting only the remaining controllable regions?

We are thus led to consider several methods for measuring the surface area of "interfaces" anticipating that we might obtain results which depend on the definition. For these considerations, it is useful to refer to Fig. 9, which is a sketch of what might happen when $\Sigma = 0$, and Fig. 10, which is a representation of what might happen for $\Sigma \neq 0$.

Configurations are shown for each of the four boundary combinations: the circles enclose regions of "frozen spins" — those that are constant under all four BCs — with solid lines indicating broken (unsatisfied) bonds. The dashed lines indicate the location of a frozen cluster embedded in a set of like spins. The interior of the configurations in Fig. 10 are also frozen. Note that the frozen spin regions can contain nested subclusters of alternating spins. In Fig. 9, spins outside of the frozen spin regions can be either $+$ or $-$, depending on the BC combination. These two figures are caricatures of configurations such as those shown in Fig. 1. Note that Fig. 9 does not show all of the possibilities. Also, these pictures are two-dimensional slices, which hides the possibilities of regions having three dimensional "handles" and minimizes the potential role of simultaneous percolation of $+$ and $-$ spins in some regions.

## B. Surface exponent $d_s$

The first method of defining an interface uses just two different boundary conditions, for example, the $+-$ to $++$ comparison. This change in boundary conditions causes a connected set of spins anchored to the right face to flip from up to down along with the forced right boundary spins when the $++$ boundaries are replaced with $+-$. This set of *changing* sites, which we denote $\mathcal{C}_{+-,++}$, has a bounding surface — indicated by the heavy and light lines in Fig. 11, for the spin configurations of Fig. 9. But some of this boundary will surround islands of fixed up spins (some of which themselves have down spin inclu-
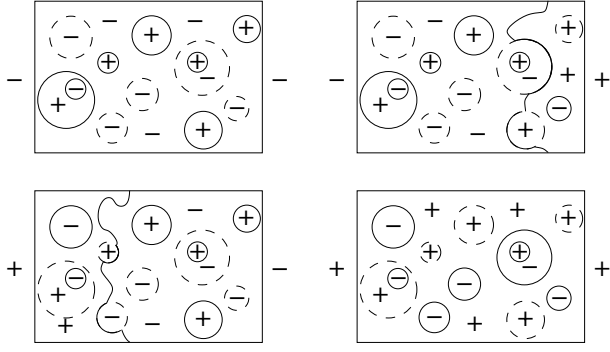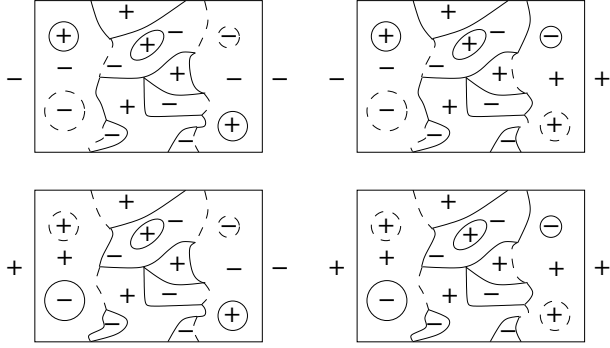
FIG. 9: Schematics of the spin configurations for four different boundary condition combinations, for a case with $\Sigma \neq 0$. Here, there is a set of *controllable spins*, connected across the sample, that can be either $+$ or $-$, depending on the boundary conditions. These are the majority of the spins in the figure shown. The *frozen spins* are those that are constant under the four boundary conditions $--$, $-+$, $+-$, and $++$; these are indicated here by the circular regions. Solid lines separate spins of opposite sign, while the dashed lines indicate frozen islands that are of the same sign as the surrounding spins.



FIG. 10: Schematics of the spin configurations for four different boundary condition combinations, for a case with $\Sigma = 0$. In addition to the frozen islands, shown as circles as in Fig. 9, there is a set of frozen interior spins that spans the sample in the directions perpendicular to the horizontal (control) axis. Conventions for solid and dashed lines are as in Fig. 9. The surfaces used to measure $d_s$ are the two surfaces of the frozen interior, but the measure used to compute $d_I$ is *zero*, as long as the boxes have side $B$ smaller than the size of the frozen interior. Also zero is the exchange stiffness $\Sigma_J$, as each bond that is broken in both the $+-$ and $-+$ configurations is also broken in both the $--$ and $++$ configurations, while bonds that are broken exactly once under one of the two antiparallel BCs is likewise broken exactly once under parallel BCs, so that all broken bonds *cancel* in the signed sum that defines $\Sigma_J$.
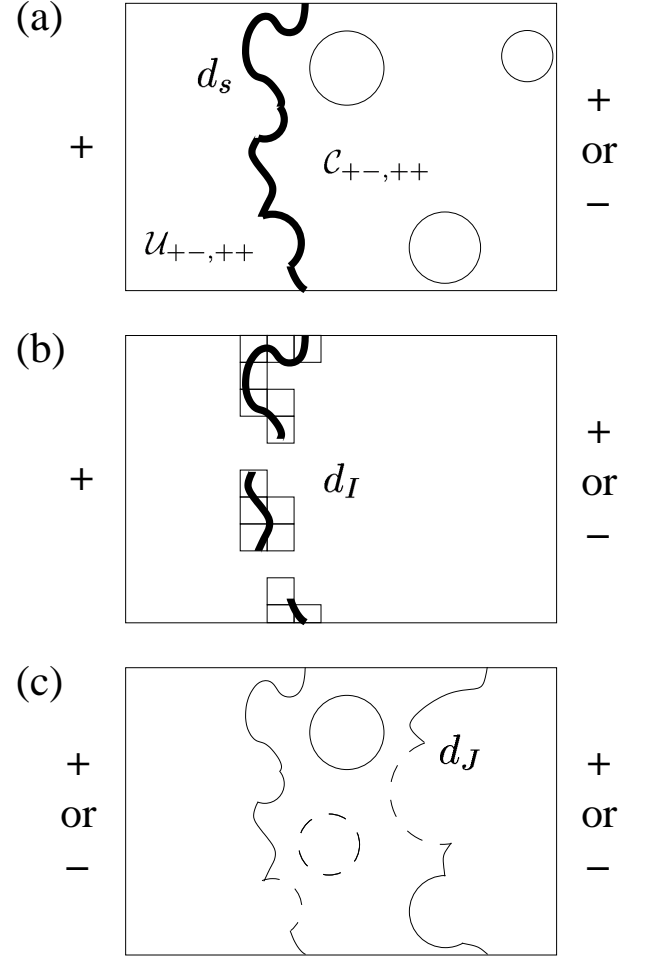


FIG. 11: Schematics of the definitions of domain wall measures, based on the configurations of Fig. 9. (a) The heavy solid lines indicate the boundaries used to define the domain walls for the calculation of the fractal dimension $d_s$ of the spanning wall obtained by comparing the $+-$ and $++$ configurations. The region of changed spins connected to the right face is $\mathcal{C}_{+-,++}$, which has both the heavy and light lines as boundary, while the unchanged connected region anchored on the left face, with the single solid line as boundary, is $\mathcal{U}_{+-,++}$. (b) Boxes used for determining $d_I$, the dimension of the locally incongruent regions. The number of boxes of side $B$ in which the $+-$ configuration differs from *both* the $++$ and $--$ configurations scales as $L^{d_I}$. The broken bonds around the frozen islands in the $++$ or $--$ configurations are not counted. (c) The signed sum of broken bonds that defines $\Sigma_J$, the exchange contribution to the stiffness $\Sigma$. Solid lines indicate positive contributions and the long dashed lines indicate negative contributions.

sions) that are disconnected from both controlled faces. The number of such islands (light circles in Fig. 11) will scale with the volume of the $\mathcal{C}_{+-,++}$ region and their boundaries will contribute an amount of order this volume to the surface area of $\mathcal{C}_{+-,++}$. This internal contribution to the surface area will, on average, be dominant in large systems when $h < h_c$, but it is clearly *not* prop-

erly part of the domain wall.

What we are interested in is the part of the boundary of $\mathcal{C}_{+-,++}$ which interfaces with the other "half" of the system. One way to define a domain wall is thus to start at the unmodified *left* face and find the set of spins connected to this face that do not change when the boundary conditions on the *right* face are changed; this

set, which we denote $\mathcal{U}_{+-,++}$, is simply connected, i.e. it has no interior holes, although it could have handles. The surface of the set $\mathcal{U}_{+-,++}$ is just its interface with the set $\mathcal{C}_{+-,++}$ that flips. This $\mathcal{U} - \mathcal{C}$ interface, which spans the whole cross-section with no holes and thus includes some boundary of frozen regions, is our first definition of a domain wall of interest.

Averaging over samples at fixed $h$ gives a mean surface area of this $\mathcal{U} - \mathcal{C}$ domain wall, $A(h, L)$. (For these and related studies, we used $5 \times 10^3$ to $20 \times 10^3$ samples for smaller sample sizes, $8^3$ through $64^3$, and $300$ to $5 \times 10^3$ samples for the largest sample size, $128^3$.) Estimates of the dimension of these surfaces, $d_s$, can be obtained from the discrete logarithmic derivative,

$$\tilde{d}_s(h, L) = \ln[A(h, \sqrt{2}L)/A(h, L/\sqrt{2})]/\ln(2). \quad (31)$$

A plot of these estimates, with statistical errors, are shown in Fig. 12. The estimates for the case of $h = 2.27 \simeq h_c$ appear to approach a fixed value, $d_s$, as $L \to \infty$, while $\tilde{d}_s \to 2$ for $h < h_c$, as expected. For $h > h_c$, the apparent exponent either starts at $\tilde{d}_s > d_s$ and falls, or first rises before dropping with $L$. This behavior presumably arises for $L \ll \xi$, where the growing volume allows for larger surface area, while for $L \gg \xi$, the domain walls become confined to a distance less than $\xi$ from the right and left faces of the sample and thus effectively become two dimensional. From this plot and the results for the (111) orientation (Fig. 17), we estimate

$$d_s = 2.30 \pm 0.04, \quad (32)$$

where systematic errors due to finite size effects and uncertainty in $h_c$ dominate the statistical uncertainties.

## C. Roughness in the ferromagnetic phase

We have verified that the surface roughness of the non-fractal domain walls in the ferromagnetic phase are consistent with theoretical expectations.[37,38,39,40] Specifically, we calculated the "height" of the surfaces — deviation from flat — in anisotropic samples of shape $X \times L^2$, with the outer two layers in the $x$-direction fixed to be $+$ or $-$ and, as before, the sample periodic in the $y$ and $z$ directions. Again, to reduce lattice artifacts, we use samples whose "$x$" faces are oriented in either the (100) or (111) directions.

As overhangs are possible in these interfaces, it is necessary to define carefully the "height" function, $u(y, z)$,: for a given $y$ and $z$ coordinates, we use twice the average of the $x$-coordinates of the set of spins in $\mathcal{U}_{+-,--}$ ; in the absence of overhangs, this gives the desired surface height. The sample averaged rms *width* $W$ is defined by $W^2 = \overline{[u^2] - [u]^2}$, where the square brackets indicate the average of $u(y, z)$ over the $y-z$ coordinates of the sample. Simple scaling in the ordered phase suggests that
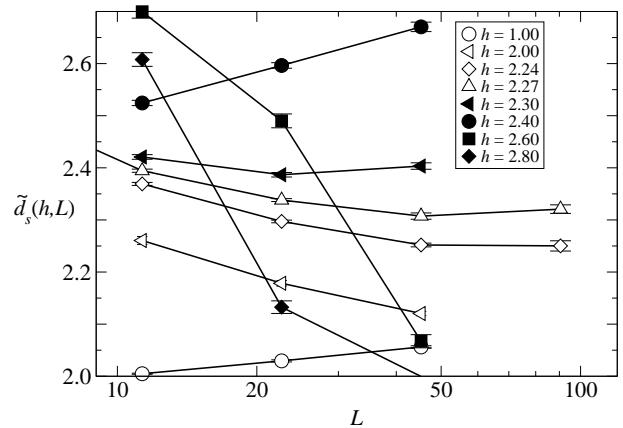
$$W = L^{\zeta} T(h, X/L^{\zeta}), \quad (33)$$



FIG. 12: Effective dimensions $\tilde{d}_s(h, L)$ obtained from a logarithmic derivative of the surface area with respect to $L$. These are used to estimate the fractal dimension $d_s \equiv \tilde{d}_s(h_c, \infty)$. The values $\tilde{d}_s(h, L)$ are calculated from the surface of the connected set of spins rooted at one face that is unchanged when the spins on the *opposite* face of the sample are flipped. The scaling of the area of this surface with $L$ yields the estimates shown, via Eq. (31). The error bars represent $1\sigma$ statistical uncertainties. The values converge to $d_s = 2.30 \pm 0.04$ for $h$ near $2.27 \approx h_c$, with the error reflecting the uncertainty in $h_c$ and the estimated magnitude of finite size corrections. The lines connect data points with the same $h$.
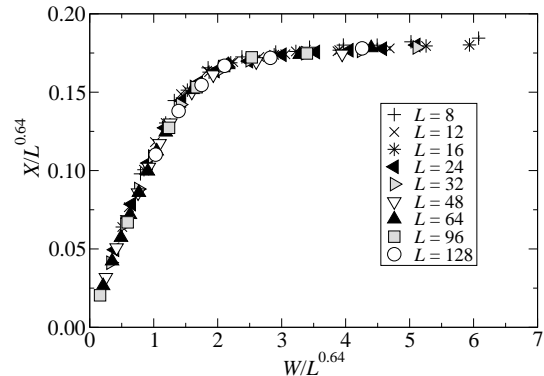


FIG. 13: Scaling plot for the roughness of a forced interface in the ferromagnetically ordered phase as a function of the aspect ratio of an $X \times L \times L$ sample. For the values of $h$ shown here with $h < h_c$, the width of the interface scales as $W \sim L^{\zeta}$ with the best fit $\zeta = 0.64(3)$, comparable to the expected exact result $\zeta = 2/3$. The statistical $1\sigma$ error bars are $1/5$ of the symbol sizes or less.

for large values of $X$ and $L$, with $T$ a geometry dependent function. We find that using $\zeta = 0.64 \pm 0.03$, consistent with the expected value[37] $\zeta = 2/3$, describes the data fairly well, as seen in Fig. 13.

The convergence of the roughness of the interface to its asymptotic form is made more apparent by defining an effective scale dependent roughness exponent

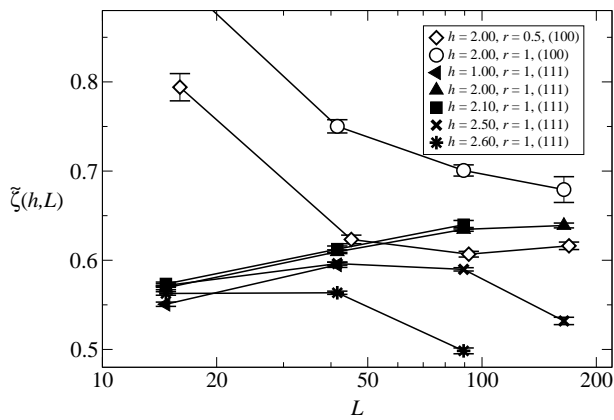$$\tilde{\zeta}(h, (L_1 L_2)^{1/2}) = \ln(W_2/W_1)/\ln(L_2/L_1) \quad (34)$$

FIG. 14: Plot of the effective roughness exponent $\tilde{\zeta}(h, L)$ in the ordered phase, for $h = 2.0$ with (100) oriented faces, and $h = 1.0, 2.0, 2.1, 2.4$, with (111) oriented faces. The samples have $X = rL^{2/3}$ layers (of area $L^2$ for (100) and area $\sqrt{3}L^2$ for (111).) For all samples in the ordered phase, the exponent approaches $\zeta = 0.66 \pm 0.03$ as $L \to \infty$, consistent with the expected $\zeta = 2/3$. For comparison, data for the disordered phase is included; the apparent exponent decreases for large systems when $h > h_c$.

where the $X_{1,2}$ are chosen to have the values $rL_{1,2}^{2/3}$, with $r$ fixed at close to unity. Assuming that $\zeta$ is indeed *near* $2/3$, this choice ensures that a typical wall is found, rather than the best of a set of $\sim L^{1-\zeta}$ possibilities that would result from using a sample that was much longer than $L^\zeta$ in the $x$ direction. Such a sample shape would result in the same asymptotic value for $\zeta$, but would have (probably logarithmic) corrections to scaling. As can be seen in Fig. 14, the effective exponent appears to converge to $\zeta = 0.66 \pm 0.03$ in both geometries. Note that even with the appropriate anisotropic scaling, the corrections to scaling are large for samples up to $L = 100$ with the corresponding $X \sim 20$.

## D. Incongruence box-counting interface exponent $d_I$

For an alternative measurement of the dimension of the domain walls at criticality, we have used a *box counting* method. In this method, we compare the configuration given $+-$ (or $-+$) boundary conditions with *both* $++$ and $--$ configurations. This is done at various scales $w$, by partitioning the sample into $(L/B)^3$ cubes of volume $B^3$. If the configuration with twisted boundary conditions differs from *both* $++$ and $--$ in a given volume $B^3$, that cube must intersect the domain wall. But this wall will *not* include any boundary of frozen regions that is isolated from other broken bonds by a distance of at least $B$. In particular, when $\Sigma = 0$, the number of such intersecting boxes $N(B, L, h)$ will be *zero* for $B$ smaller than the size of the frozen interior region. For example, the $+-$ and $-+$ configurations in Fig. 10 are *locally*
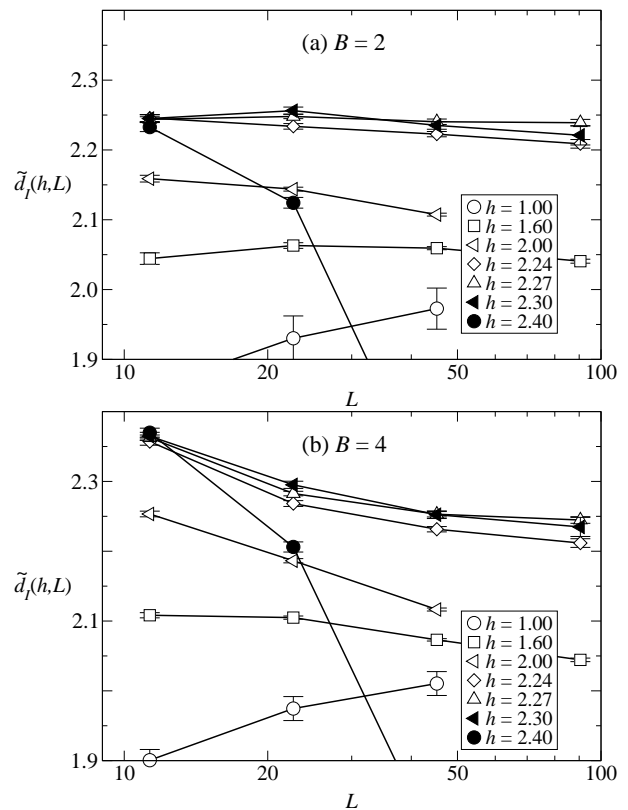


FIG. 15: Estimates $\tilde{d}_I(h, L)$ of the box-counting fractal dimension $d_I = \tilde{d}_I(h_c, \infty)$, for the (100) orientation of controlled faces. Comparisons of the $+-$ configuration are made with the $--$ and $++$ configurations in boxes of volume $B^3$. If the $+-$ configuration differs from both of the others, that box is considered part of the domain wall. The finite logarithmic derivative of the scaling of the number of such boxes with sample size $L$ yields the estimates shown with the lines connecting data points with the same $h$. The error bars represent $1\sigma$ statistical uncertainties. For $h = 2.27$, the dimension estimate converges to $d_I = 2.24 \pm 0.03$, the error being a combination of statistical error and systematic errors ($\approx 0.02$) caused by finite size effects and uncertainties in $h_c$.

congruent everywhere with either the $--$ or the $++$ configuration. Thus only for boxes larger than the width of the interior region will a domain wall be apparent.

The scaling of the number of intersecting boxes $N(B, L, h)$ with $L$ gives an alternate estimate of an effective fractal dimension which we call $d_I(h, L)$, anticipating that $N \sim (L/B)^{d_I}$ at the critical point (see Fig. 11(b).) Using the same form of the discrete logarithmic derivative between scales $L$ and $2L$ as in Eq. (31) gives the effective exponent $\tilde{d}_I(h, L)$, as summarized in Figs. 15 and 17. This estimate yields a constant at large $L$, within statistical errors, for $h = 2.27 \simeq h_c$ and gives a value $d_I = 2.24 \pm 0.03$.

We note that a useful compatible definition for $d_I$ can be based on *bonds* rather than spin blocks: count the number of bonds that are broken with the $+-$ or $-+$ BCs that are satisfied with both the $++$ and $--$ BCs.

The number of such bonds $N'$ should have the same scaling form as $N$ does for fixed $B$. We have used this bond definition in a smaller number of samples and find results for $\tilde{d}_I(h, L)$ at large $L$ consistent with the spin block definition of $d_I$ defined above.

### E. Exchange stiffness exponent $d_J$

A third measure that we have used to study domain wall geometry is the contribution of the *exchange energy* to the stiffness $\Sigma$. This we denote $\Sigma_J$. It is the *signed sum* of the broken bond weights, counted as negative for the $--$ and $++$ configurations and positive for the $-+$ and $+-$ configurations.

As in computing $\Sigma$, using the symmetrized energy differences reduces boundary effects. If $\Sigma = 0$, then $\Sigma_J = 0$, for example, though comparing the configurations with $++$ and $+-$ boundary conditions in such a sample will reveal a domain wall while comparing those with $++$ and $-+$ boundary conditions will reveal a second entirely distinct domain wall. Either of these domain walls, along with a portion of the frozen spins that make up the boundary, would be counted in the method which yielded $d_s$. But in this symmetrized measure from $\Sigma_J$, the signed sums would cancel, so that neither domain wall would be counted. Similarly, when the box size $B$ is smaller than the size of the frozen interior, the measure used to find $d_I$ would also be zero. Note, however, that $\Sigma_J$ *does* include some of the boundaries of the frozen regions but it does so with signs that can be either positive or negative. In the ordered phase, then, the exchange stiffness $\Sigma_J$ will include contributions from the region between the two domain walls that occur, contributions that would not have been included in the other methods. The three proposed measures are thus potentially all different, especially off-critical, but perhaps also at criticality.

At the critical point the exchange energy part of the symmetrized stiffness will have contributions from the domain walls with holes, $\sim L^{d_s - \beta/\nu}$, equivalent to the box counting measure of the domain wall, as well as contributions from parts of the boundaries of the frozen regions. The simplest expectation is that the the contributions from the frozen region boundaries will be random in sign and thus less important *in toto*.

The mean of $\Sigma_J(h, L)$ can be used to compute a fractal-dimension-like quantity, $d_J$, for the interface via the assumption that $\overline{\Sigma}_J \sim L^{d_J}$ at $h_c$. The scale dependent effective exponents from our data at $h = 2.27$, shown in Fig. 16, yield an estimate of $d_J = 2.18 \pm 0.02$ that appears to be slightly smaller than the other two dimensions $d_s$ and $d_I$.

One advantage of the exchange energy is that we can relate this measure of the fractal dimension of the domain walls at the critical point to the other exponents. If a small additional exchange $\delta J$ is added to the Hamiltonian (or equivalently if all the random fields were decreased in magnitude by a uniform small amount) then the change
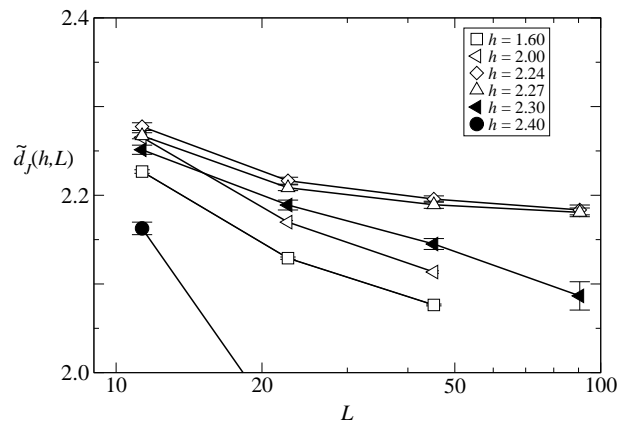


FIG. 16: Estimates $\tilde{d}_J(h, L)$ of the scaling of the exchange contribution to the stiffness defined as the total signed surface area of the changes between $++$, $--$, $-+$ and $+-$ boundary conditions. The logarithmic derivative of $\overline{\Sigma}_J(L)$ gives the values shown with the lines connecting data points with the same $h$. The error bars represent $1\sigma$ statistical uncertainties. For $h = 2.27$, the dimension estimate converges to $d_J = 2.18 \pm 0.03$.
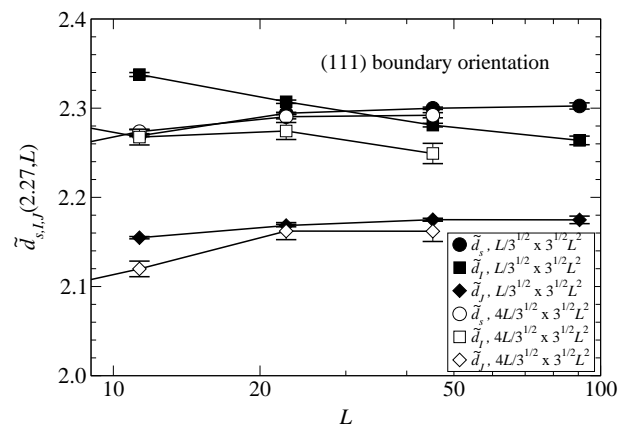


FIG. 17: Estimates $\tilde{d}_s(h = 2.27, L)$, $\tilde{d}_I(h = 2.27, L)$, and $\tilde{d}_J(h = 2.27, L)$ of the fractal dimensions using controlled boundary surfaces in the (111) plane of the cubic lattice which are rhombi with sides of $L$ spins. The number of layers in the sample, including the boundary planes, is $L$ or $4L$, as shown in the key. The error bars represent $1\sigma$ statistical uncertainties with the lines connecting data points with the same $h$. The dimension estimates converge to $d_s = 2.30 \pm 0.02$, $d_I = 2.25 \pm 0.05$, $d_J = 2.18 \pm 0.03$; these are consistent within errors with those from Figs. 12, 15, and 16.

in the stiffness would be simply

$$\delta \Sigma \approx \frac{\delta J}{J} \Sigma_J. \tag{35}$$

Since $\Sigma \sim L^\theta$ while $\Sigma_J \sim L^{d_J}$ with $d_J > \theta$, the change in the stiffness will become of order the stiffness itself and thus strongly modify the system when $L \sim (\delta J)^{-1/(d_J - \theta)}$. This crossover length is thus a measure of the correlation length, $\xi$, and we thus expect the

exponent equality

$$\frac{1}{\nu} = d_J - \theta. \tag{36}$$

This can be derived directly from the scaling form Eq. (25) by differentiating with respect to $J$ (equivalently with respect to $-h$) and noting the thermodynamic identity between derivatives with respect to coefficients of terms in the Hamiltonian and expectations of the corresponding term. (Note that this is closely analogous to the relation between $\nu$ and the energetic part of the interfacial free energy at conventional finite temperature critical points.) Assuming the scaling relation Eq. (36) would give $\nu = 1.45 \pm 0.10$, a slightly different, but consistent, value of $\nu$ than that from the scaling of the total symmetrized stiffness $\Sigma$.

### F. Comparison of domain wall exponents

Due to the subtleties introduced by frozen islands and the representation of the Hamiltonian as the sum of domain wall and random field components, there are three natural measurements of the domain wall surface and the domain wall contributions to the stiffness. Each measure has its own physical meaning. We will argue in Sec. IX B that the difference between $d_s$ and $d_I$ is due to frozen islands, and hence $d_s - d_I$ should be related to $\beta/\nu$.

## VII. MAGNETIZATION

Having established the location and order of the transition, we now focus on an apparently problematic quantity: the magnetization. Given sets of ground state spin configurations $\{s_i\}$, the distribution of magnetizations can be studied as a function of $L$ and $h$. In order to better understand the large volume limit, we have computed the magnetization distributions for *five different boundary conditions*: all boundary spins fixed to a single value, either all positive or all negative ($F$); boundary spins fixed at independent random values ($R$); open boundary conditions ($O$); periodic boundary conditions ($P$); and a combination ($Q$) with conditions $P$, $O$, and $R$ along each of the three axes . The fixed spin boundary conditions will tend to favor ferromagnetism, the random will tend to favor a disordered phase and the combination $Q$ appears to significantly reduce some finite size effects.

We first describe our results for the mean of the absolute value of the magnetization density

$$|m| = |\sum_i s_i|L^{-d} \tag{37}$$

for cubic samples with periodic boundary conditions (P). Fig. 18 is a plot of our data as a function of $h$, for various $L$; the magnetization drops off quite steeply near $h_c$. Fig. 19 shows the magnetization as a function of system
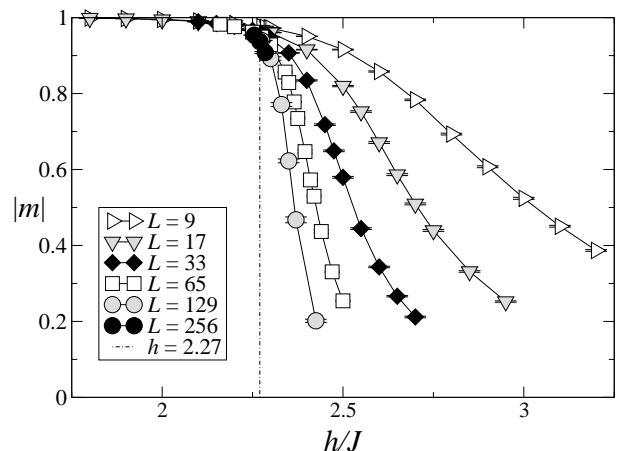


FIG. 18: Mean absolute magnetization per spin, $|m|$, plotted vs. $h$ for various $L$, for periodic boundary conditions.

size, along with its discrete logarithmic derivative, which yields an effective scale dependent exponent. To within errors, the magnetization is consistent with power law scaling,

$$m \sim L^{-\beta/\nu}, \tag{38}$$

with $\beta/\nu = 0.012 \pm 0.004$. For $h < h_c$, the magnetization appears to approach a constant (e.g., $m(2.255, L \to \infty) \approx 0.952$). For $h > h_c$, the effective exponent decreases significantly as $L$ increases.

For further analysis, we characterize the distributions of $m$ by the average over samples of the square of the magnetization per spin, $\overline{m^2}$, and the root-mean-square sample-to-sample variations of the square of the magnetization

$$\Delta_{m^2} \equiv \sqrt{\overline{m^4} - (\overline{m^2})^2}. \tag{39}$$

Our results for $\Delta_{m^2}$ are shown in Fig. 20. As $L$ is increased, the peak magnitude of $\Delta_{m^2}$ is seen to decrease for some boundary conditions $F$, $O$ and $P$, while it increases for others $R$ and $Q$. For boundary conditions $R$, $O$, $P$, and $Q$, the peak heights appear to be converging to a similar fixed value, bracketed from above and below by the different sets of data. In general, we would expect that the height of these peaks would scale for asymptotically large sizes as $L^{-2\beta/\nu}$; the data are thus consistent with either $\beta = 0$ or with a very small $\beta$.

One can estimate the location of the transition by fitting the data for $\Delta_{m^2}$ near the peaks at five or more values of $h$ to a Gaussian form. (The Gaussian gives a better fit than a parabolic form over a larger range of $h$, though either form should give the same limit for $h$ near enough to the peak and $L$ large enough.) The fitted location of the peaks is extrapolated for all boundary conditions as a function of $L$. We obtain agreement of the extrapolations for $1.3 < \nu < 1.45$ with a value of $h_c = 2.272 \pm 0.004$, consistent with the value from $P_0$ and other estimates. We believe that this independent
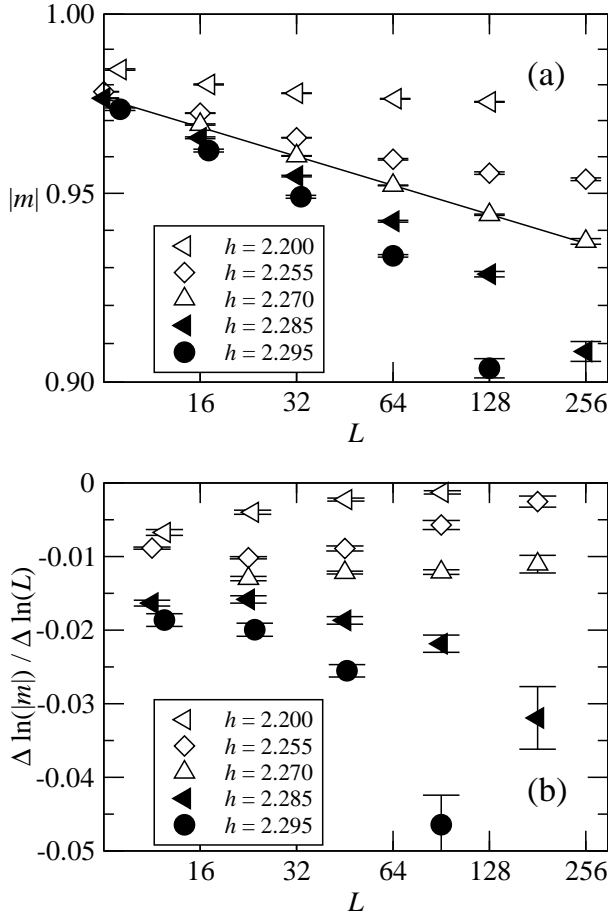
FIG. 19: (a) Mean absolute magnetization per spin, $|m|$, plotted vs. $L$ for various $h$ (with periodic boundary conditions.) The solid line is $|m| = (1.0009)L^{-0.012}$. (b) The discrete logarithmic derivative $\Delta \ln(|m(L)|)/\Delta \ln(L) \equiv \ln(|m(L')|/|m(L)|)/ln(L'/L)$, vs. $\sqrt{LL'}$, with $L' \approx 2L$. This is used to directly estimate $\beta/\nu$, yielding $\beta/\nu = 0.012 \pm 0.004$, where the error bars are dominated by the range of values for $h_c$ obtained by fitting over sizes up to $L = 256$.

estimate is relatively precise and robust, due to the variety of boundary conditions used, with the variation in the results giving an estimate of systematic uncertainties.

For the fixed spin boundary conditions, $F$, the peak magnitude of $m^2$ is apparently converging to a *different* value (note that the magnetization near the surfaces will vary less than with the other boundary conditions.) If either these data, $F$, or the periodic boundary condition data, $P$, *at the critical point* are used (rather than the data near the peak) then a smaller value of $\Delta_{m^2}$ is found, roughly the same although apparently still distinct for these two cases.

Collectively, our magnetization data would appear to suggest a picture of the transition that is consistent with that of reference Ref.13: three possible "states" at the critical point, "up", "down", and "disordered" as would occur at a first order para- to ferro- magnetic transition. As we shall see, however, our other data and further
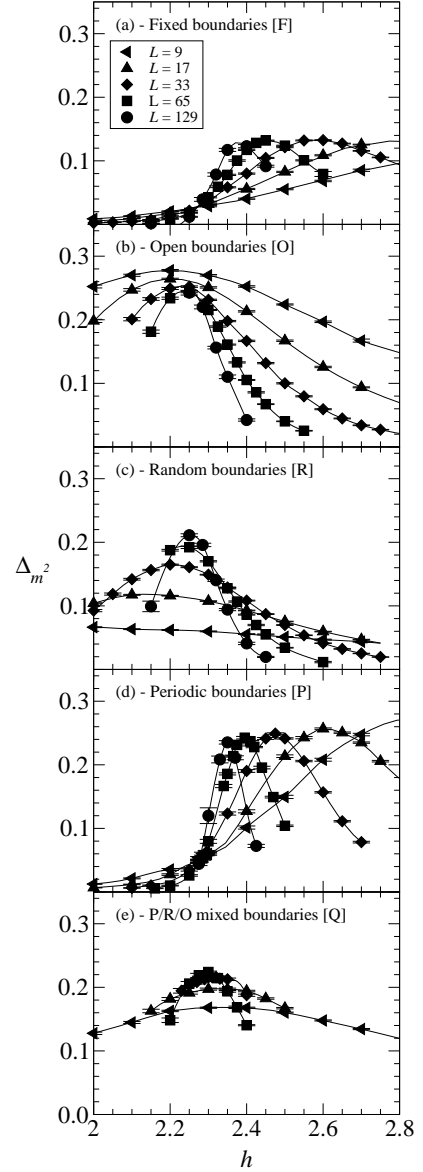


FIG. 20: Magnitude of sample-to-sample fluctuations $\Delta_{m^2}$ in the mean square magnetization per spin, as a function of random field strength $h$, for various system sizes, $L$, (a) for fixed $s_i = +1$ boundary conditions $(F)$, (b) for open (free) boundary conditions $(O)$, (c) for random fixed spin boundary conditions $(R)$, (d) for periodic boundary conditions $(P)$, and (e) for mixed periodic, random fixed, and fixed boundary conditions, one along each axis $(Q)$. The curves are fit locally with Gaussians in the regime where $\Delta_{m^2}$ is greater than approximately 3/4 of its peak value. Extrapolating the peak locations to $L = \infty$ gives a best fit value of $\nu = 1.38 \pm 0.08$ and $h_c = 2.272 \pm 0.004$, with the dominant errors being systematic errors arising from variations in the extrapolated values, presumably due to corrections to scaling. The lines shown are spline fits to visually organize the data.

thought suggest that this picture, while a very good approximation, is not correct. We will argue that in fact $\beta$ is small but non-zero and thus in astronomically large samples the magnetization will decay slowly to zero at the critical point but with the scaling functions for the distribution of the magnetization (and their moments) depending on the type of boundary conditions as is the case for pure systems at conventional critical points.[42] Data suggesting this is presented in the next section.

## VIII.  SPIN CLUSTERS AT CRITICALITY

The distribution of the magnetization studied above gives some information about the ground state correlations of the RFIM. But because ground state correlations between Ising spins are controlled by the probability that a pair of spins of interest are in opposite directions, the observation that the magnetization at the critical point tends to be rather close to saturation suggests that the loss of correlations as the random field is increased through the critical point may be associated with rather rare events. In this section, we investigate the nature of the effect that we believe gives the dominant contribution: the occurrence of connected clusters of spins of the one sign completely surrounded by spins of the opposite sign. Because all of the exchanges are ferromagnetic, such *isolated inverted clusters* will, *a fortiori*, not change when the boundary conditions are inverted: either the spins surrounding them will flip in which case they will be content the way they were, or the surrounding spins will not flip and the spins in the cluster will be isolated from the boundary condition change. Thus these isolated spin clusters are frozen.

We have computed the statistics of the domain walls that enclose isolated spin clusters in 5000 or more samples of system sizes up to $128^3$ and 1000 samples of size $256^3$ at $h = 2.27 \approx h_c$. A slice of a configuration is shown in Fig. 21. Statistical errors in the dimension estimates and number distribution were computed by a bootstrap method (resampling the statistics over the computed configurations);[43] the error bars indicate the estimated rms fluctuations in the statistics at each cluster size.

We note that previous work by Esser, Nowak and Usadel[44] studied the domain structure for a single sample size. They address questions of percolation in the 3D Gaussian RFIM, but they claim that the cluster distribution is not broad. We find, in contrast, that there is a broad tail, which, though weak for smaller systems, becomes more important as $L$ increases at the critical point. To directly contrast with the results of Ref.44, we find that the sum of the volume fraction of the *two* largest clusters, though near 1, slowly *decreases* as $L$ increases, at $h = 2.27 \approx h_c$. The transition separates a state with one infinite connected set of spins of the same sign from a disordered state with two antiparallel incipient infinite clusters.
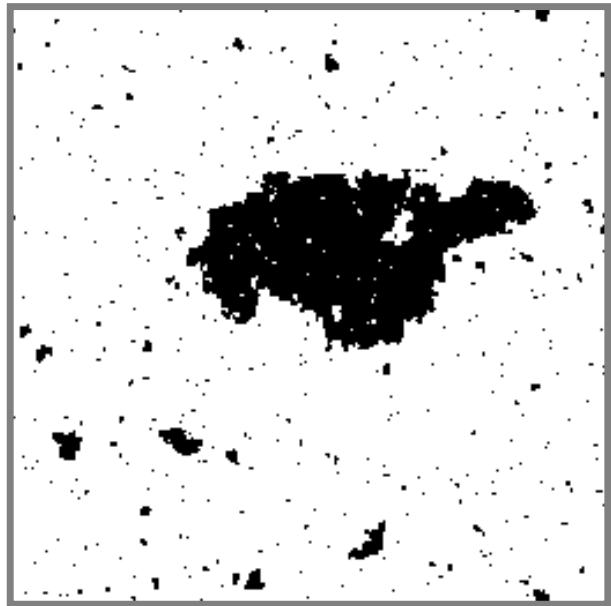


FIG. 21:  A slice of a spin configuration in a $256^3$ sample at $h = 2.27$. The dark squares indicate an up spin. The nesting of spin clusters can be seen here — the number of levels of nesting, the "depth", of the full configuration is $k = 3$. The domain walls are determined by working recursively inwards from the majority (down) spin cluster. The surface of each cluster is taken to be the outer surface and does not include the surface of subclusters.

### A.  Cluster surface

For each cluster, the total volume, $v$, — which includes the volume of "holes" of opposite spin — was computed, as was the surface area, $a$, of the cluster: the number of unsatisfied nearest neighbor bonds that separate the cluster from its *surrounding* region of opposite spin. The domain walls are found recursively, taking as the initial surrounding region the majority spin cluster, which typically occupies $> 97\%$ of the volume at $h_c$ for $L < 256$.[45] Binning the clusters by volume $v$, logarithmically spaced by powers of 2, averaging the surface area in each bin, and taking the discrete logarithmic derivative gives an estimate of the fractal dimension of the cluster surfaces, dimension $\tilde{d}_s^c(h, L, v)$. As indicated in Fig. 22, at the critical point the surface area appears to scale as $v^{0.755 \pm 0.07}$ for intermediate size clusters with $1 \ll v \ll L^3$. The error in this exponent includes both statistical error and the apparent uncertainty of corrections to scaling that are affecting the convergence to a constant value. This value is little affected by the estimate of the location of $h_c$ (varying $h$ changes the number of clusters, but, within the uncertainty of $h_c$, does not affect the geometry of the domain walls.) We have verified that the volume enclosed by the domain walls separating opposite spins scales in a manner numerically consistent with this *volume* being *nonfractal*:
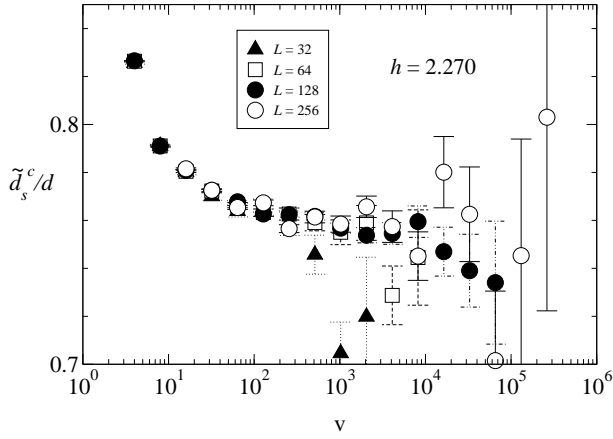
$$v \sim \ell^d, \tag{40}$$

FIG. 22: Dependence of the surface area (number of broken bonds) of cluster boundaries on the enclosed volume, $v$, expressed as an effective exponent $\tilde{d}_s^c(h, L, v)$, at $h = 2.270 \approx h_c$, for $L = 32, 64, 128, 256$. The cluster surface area scales as $v^{0.755 \pm 0.007}$ for the largest clusters that are not affected by finite size effects, yielding a fractal dimension $d_s^c = 2.27(2)$ for the cluster surfaces.

with $\ell$ being either the geometric mean or the maximum of the lengths of the sides of the minimal rectilinear box that encloses the cluster. The extrapolation of $d_s^c(h, L, v)$ to large $L$ and $\ell$ is therefore consistent with clusters having typical diameter $\ell \sim v^{1/d}$ and typical surface area

$$a \sim \ell^{d_s^c} \qquad (41)$$

with

$$d_s^c \simeq 2.27 \pm 0.02 \qquad (42)$$

a fractal surface dimension consistent within the statistical uncertainties with our estimates of the fractal dimensions $d_s$ and $d_I$ of the domain walls induced by changing boundary conditions at the critical point. In particular, this surface dimension bears a close resemblance to the dimension of the spanning surface which we denoted $d_s$; thus we conjecture that

$$d_s^c = d_s. \qquad (43)$$

## B. Cluster density

New information is given by the *densities* of the clusters as a function of their size, in particular their dimensionless volume fraction

$$\rho(v) \equiv \frac{v}{\delta v} \text{Prob[site} \in \text{cluster of size in } (v, v + \delta v)]. \quad (44)$$

From the data in Fig. 23 (and for the slightly different measure of Fig. 24, where $v$ is the volume of the smallest parallelepiped of fixed orientation enclosing the cluster) we see that clusters that are neither too small nor limited by finite size effects — roughly a decade in length
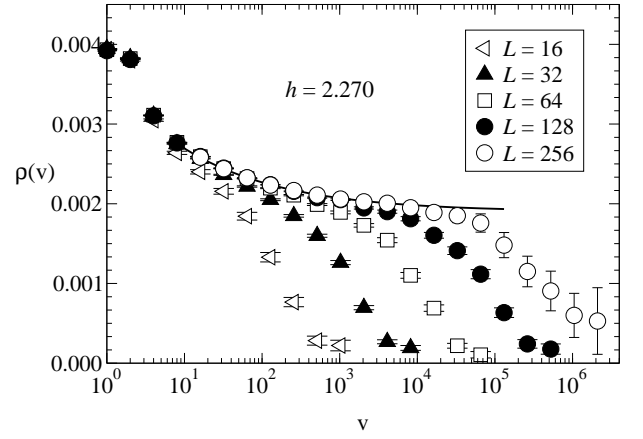


FIG. 23: Fraction of the volume $\rho(v)$ occupied by clusters of volume between $v$ and $ev$, at $h = 2.270 \approx h_c$, found by normalizing the data binned according to powers of 2 (i.e., dividing the volume fractions in the $[v, 2v]$ bins by $\ln 2$.) The solid line is $\rho(v) = 0.0019 + (0.0017)v^{-0.33}$, one of the trial fits used to extrapolate to large $v$.
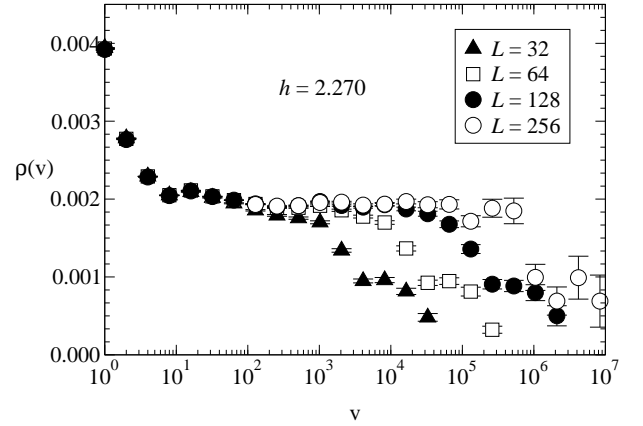


FIG. 24: Fraction of the volume $\rho(v)$ occupied by clusters that are contained in *rectilinear volumes* ("boxes") between $v$ and $ev$, at $h = 2.270 \approx h_c$, found by normalizing the data binned according to powers of 2 (i.e., dividing the volume fractions in the $[v, 2v]$ bins by $\ln 2$.) For large $v$, $\rho(v) \to 0.0019 \pm 0.0002$, if $h_c = 2.270$.

scale for $L = 256$ — occupy an approximately scale independent volume fraction. A comparison of the cluster distributions for nominally off-critical values of $h$, as seen in Fig. 25, shows how $\rho(v)$ depends on $h$. From these plots we infer a large-$v$ limit of

$$\rho(v) \to \rho_\infty \simeq 0.0019 \pm 0.0004. \qquad (45)$$

We cannot, of course, rule out a slow decrease of $\rho(v)$ to zero for large volumes, especially as our effective range of length scales here is less than for other quantities because of the restrictions due to finite size effects. But we *can* understand on the basis of our other observations why one should expect a small but non-zero value for $\rho_\infty$.
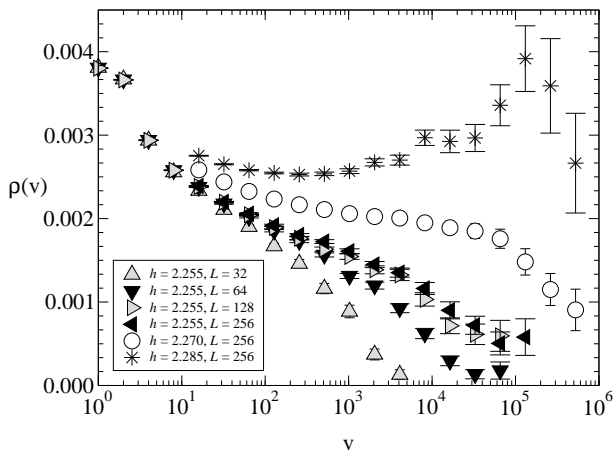
FIG. 25: Fraction of the volume $\rho(v)$ occupied by clusters of volume between $v$ and $ev$, found by normalizing as in Fig. 23. Here, the volume fractions are plotted for $L = 32, 64, 128$, with $h = 2.255$, and $L = 256$, with $h = 2.255, 2.270$ and $2.285$, to indicate some of the effect of changing $L$ or $h$ on $\rho(v)$. The data for $h = 2.255$ apparently converges at large $L$ to a well defined distribution that has a finite-$v$ cutoff, consistent with a finite correlation length in the ordered phase. This is in contrast with the data for $h = 2.27$, the putative critical point, for $L \leq 256$, as seen in Fig. 23. For $h = 2.285$, in the disordered phase, large volume clusters start to occupy a larger fraction of the volume than smaller clusters, for $L = 256$.

## IX. SCALING

In this section we pull together our various results about domain walls, stiffness, magnetization, and inverted spin clusters and show how they are all consistent with a simple picture of scaling behavior at a zero temperature phase transition.

### A. Critical correlations

At the critical point, the energy cost of domain walls is typically sufficiently large that almost all cubical samples — about 96% of them — would rather have no spanning (or other large scale) domain walls unless forced to by boundary conditions. But in a small fraction of the cubical samples the random fields in the central region are sufficiently strong that they force the system to have *two* domain walls for one of the two "ferromagnetic" ($++$ or $--$) choices of boundary conditions. In samples that are twice as long, this occurs much more frequently as evidenced by the increase, on going from cubical to elongated samples, in the probability, $P_0$, that the stiffness vanishes. Although whether such a pair of walls is favorable generally depends on both the random fields in the whole system and the local behavior near the walls, a crude picture of what is going on can be drawn by assuming that the wall energies are relatively local and weakly dependent on each other. We restrict consideration for

now to the critical point.

First consider a system of dimensions $\frac{1}{2}L \times L \times L$ with the boundary conditions imposed on the faces perpendicular to the short axis. Assume that the probability that the single wall energy, $E^\ell_{+W} \equiv E_{+-} - E_{++}$, in such a system is *negative* is $q \ll 1$. Crudely, for two walls to be favorable in a cubic system with $++$ boundary conditions, as is needed to make $\Sigma = 0$, one must have *both* $E^\ell_W < 0$ for the left half of the system and $E^r_W \equiv E_{-+} - E_{++} < 0$ for the right half of the system. Naively, this occurs with probability of order $q^2$. (More precisely, one of the $E_W$'s could be positive but not by enough to dominate the other one; this will not change things much as long as the bulk of the distribution of the $E_W$'s is skewed substantially to the positive side of zero.) But in a system of length $2L$ rather than $L$, there are many more possibilities: if we divide the system into four sections of length $L/2$, one could have, for example, the second from the left having $E^\ell_W < 0$ and the rightmost having $E^r_W < 0$ with the wall energies of the other sections being positive. As there are six such choices among the four sections of the elongated system, we expect that the chances of having $\Sigma = 0$ will be about six times as large as in the cubical system — obviously a very crude approximation, but one that yields roughly the measured magnitude of the ratio $P_0(2L \times L \times L)/P_0(L \times L \times L)$. Note that this picture implies that for systems that are much longer than they are wide, the typical number of domain walls in the ground state will grow linearly with the length. The roughly random spacing between them will lead to exponential decay of the end-to-end correlations in such a system, with a characteristic length proportional to the linear dimension of the cross-section as should be expected on general finite size scaling grounds.

At conventional critical points in two dimensions, conformal invariance relates the exponential decay of correlations in long tubes to the power law decay of correlations in the bulk in infinite systems: the exponent $\eta$ is simply proportional to the ratio of the width-dependent correlation length to the width.[46] In our case, there is no such exact relation, but one can make a qualitative argument that suggests a similar result. Consider a region of diameter of order $\ell$ centered on some chosen spin in the bulk of the sample and assume that outside of this region, the spins in the vicinity are $+1$. The only way that the spins inside the region of interest can be $-1$ is if there is a domain wall relative to the pure "up" configuration which surrounds this region and has negative energy. Roughly speaking, such a closed domain wall must be made up of four or more sections which are joined together with each having negative (or close to zero) energy. Since the amount of freedom perpendicular to the area of each of these will be somewhat less than their linear dimensions, a crude approximation is that the probability of finding each such section is of order $q$ and the probability of finding the total domain wall energy negative is of order $q^4$. With $P_0[\text{cube}] \simeq 0.04 \sim q^2$, this suggests that the probability for finding such a spin flipped region will be of

order $\rho_\infty \sim q^4 \sim 0.002$, in the same range as that found. Although the above argument is very crude — factors of two's or pi's could easily have been fudged in! — it nevertheless provides a suggestive connection between the smallness of various quantities. Indeed, it actually provides more: a precise method for estimating $\beta/\nu$.

Consider a single spin in the center of a large system at the critical point with, for simplicity, $+$ boundary conditions . For each factor of $e^{1/d}$ in length scale, $\ell$, there is a probability $\rho_\infty$ that the spin is an element of a cluster, flipped with respect to its surroundings, with volume in the associated range $\ell^d \leq v < e\ell^d$. There will, of course, be correlations between the probabilities of occurrences of such inverted regions that are similar in size and nearby to one another. But, because inverted regions are so rare, the effects of these correlations will be negligible and we can assume that each range of $\ell$ around the chosen spin is independent. A simple picture of the behavior then emerges: the spin of interest will be in a cluster of one orientation of diameter $\ell_1$, which itself will be in a much larger cluster of the opposite orientation of size $\ell_2$, etc. with the successive sizes growing approximately geometrically — more precisely as a Poisson process in $\ln(\ell)$ with density $d\rho_\infty$ (with $d = 3$). The probability, $p_\parallel$, that the spin has the same orientation as the largest cluster — the system size $L$ — can readily be computed from the properties of the Poisson process; this result yields the mean value of the spin given fixed $(+)$ boundary conditions

$$\overline{s}^{(+)} = 2p_\parallel - 1 \sim \frac{1}{L^{\beta/\nu}} \qquad (46)$$

with the exponent

$$\frac{\beta}{\nu} \approx 2d\rho_\infty \simeq 0.011 \pm 0.003 \qquad (47)$$

A similar argument for two spins a distance $|x - y|$ apart in an infinite system gives

$$\overline{s_x s_y} \sim \frac{1}{|x - y|^{d-2+\tilde{\eta}}} \qquad (48)$$

with the modified "anomalous dimension" exponent for these *untruncated* zero-temperature correlations given by

$$d - 2 + \tilde{\eta} = 2\beta/\nu \approx 4d\rho_\infty. \qquad (49)$$

This picture of droplets within droplets strongly suggests that *neither* spin species will percolate at the critical point. This is, a priori, rather surprising as the percolation concentration for a three dimensional cubic lattice is substantially less than half and so one might have expected both spin species to percolate even somewhat into the ordered phase. The fact that they do not in this system is associated with the smallness of $\beta$ and the nature of the critical point.

In practice, unfortunately, the value of $\beta/\nu$ is so small for the 3D RFIM that the effects discussed above will be all-but unobservable even if experiments could reach equilibrium. But in higher dimensions, four or five, they might be observable numerically as relatively large systems sizes (e.g., more than $32^4$) can be explored.

## B. Fractal dimensions of domain walls

The picture developed above suggests that the various fractal dimensions of interfaces or domain walls at the critical point will *not* be the same but might, nevertheless, be related to the other exponents. The fractal dimension of the spanning interface $d_s$ (and the dimension of the surfaces of clusters) is the dimension of a true surface, one with no holes in it. Such a surface cuts across the whole system but the sets of sites it is separating cannot really be thought of as belonging to different states — the "up" and "down" states — since, in an asymptotically large system, most of the sites will be frozen and unaffected by the boundary conditions. In contrast, the incongruence box counting dimension, $d_I$, is sensitive only to those parts of the system that *are* affected by boundary conditions: a fraction of order $1/L^{\beta/\nu}$. A natural conjecture is that the box counting dimension is the same as that of the intersection of a typical fractal spanning surface with a fractal set of dimension $d - \beta/\nu$ yielding:

$$d_I = d_s - \beta/\nu. \qquad (50)$$

This picture is somewhat analogous to what would occur right at percolation in a diluted ferromagnetic Ising system at zero temperature: in a finite fraction of the samples, forcing a domain wall by changing the spin boundary conditions would cost no energy, while in the rest it would cost an energy proportional to the area of an interface that only cuts across the fractal incipient infinite cluster; this interface would have dimension analogous to our $d_I$.

The exchange energy dimension, $d_J$ is sensitive to both the frozen and the unfrozen regions. But a reasonable guess is that this is dominated by the unfrozen regions as the frozen regions contribute random signs. This suggests that

$$d_J = d_I = \theta + 1/\nu \qquad (51)$$

which, if correct, implies that a relation obtains between $d_s$ and the other exponents :

$$d_s = \theta + \frac{1 + \beta}{\nu}. \qquad (52)$$

We should note, however, that these conjectures are difficult to test in three dimensions, due to the smallness of $\beta$. Our estimated exponents are in slight disagreement with these conjectures, but corrections to scaling that are not apparent can be important at this level of accuracy. Nevertheless, our apparent values for $d_s$ and $d_s^c$ do appear to be larger than $d_I$ and $d_J$.

In higher dimensions, testing the conjectured scaling relations between these dimensions and the other exponents might be feasible. It is of course possible, however, that further analytic understanding would imply that at least some of the fractal dimensions could be independent exponents.

## C. Specific heat

The specific heat of the RFIM can be experimentally measured[27] and is of theoretical importance. Monte Carlo methods at finite temperature have been used to estimate its value.[12,47] In addition, Hartmann and Young (HY) have recently[26] computed the exponent $\alpha$ describing the divergence of the specific heat, using ground state configurations. They find a value of $\alpha = -0.63 \pm 0.07$. Using the *same* thermodynamic assumptions, but different analysis methods, we find $\alpha = -0.01 \pm 0.09$.

One expects[26] that the finite temperature definition of the specific heat can be extended to zero temperature, with the second derivative of $\langle E \rangle$ with respect to temperature being replaced by the second derivative of the ground state energy density $E_{\mathrm{gs}}$ with respect to $h$, or equivalently up to constants, $J$. The first derivative $\partial E_{\mathrm{gs}}/\partial J$ is just the average number of unsatisfied bonds per spin, $E_J = L^{-d} \sum_{<ij>} s_i s_j$. Hartmann and Young (HY) calculate the needed second derivative by finite differences of $E_J(h)$ for values of $h$ near $h_c$. ($E_J$ is not explicitly dependent on $J$, but changes discontinuously in a finite sample when the spin configuration $\{s_i\}$ changes; the second derivative is thus a set of $\delta$-functions which are smoothed by the finite differencing.) The finite-size scaling form assumed is that the singular part of the specific heat $C_s$ behaves as

$$C_s \sim L^{\alpha/\nu} \tilde{C}[(h - h_c)L^{1/\nu}]. \tag{53}$$

HY determine $\alpha$ by fitting to the maximum of the peaks in $C_s$, which occur at $h_{\mathrm{peak}}(L) - h_c \sim L^{1/\nu}$.

Here, we estimate $\alpha$ using the results for the stiffness from Sec. V and also by studying the behavior of $\overline{E}_J$ at $h_c$. The first estimate found by applying Eq. (6) with our values of $\theta$ and $\nu$, is $\alpha_{(1)} = -0.07 \pm 0.17$. The computation from the behavior of $\overline{E}_J$ is based on integrating Eq. (53) up to $h_c$, which gives the dependence

$$\overline{E}_{J,s}(L, h = h_c) = c_1 + c_2 L^{(\alpha-1)/\nu}, \tag{54}$$

with $c_1$ and $c_2$ constants. We have computed $E_J$ for a large number of samples of various sizes and estimated the singular part of the sample average. We directly fit our data for $\overline{E}_J(L)$, at fixed $h$, to the form Eq. (54). The fit for the nominal $h_c$, $h = 2.27$, is shown in Fig. 26. The fitted values are $(\alpha - 1)/\nu = -0.82 \pm 0.02$, *where the quoted error is purely statistical*. The fit is good for $16 \leq L \leq 256$, with $\chi^2 = 0.65$ for a three parameter fit to five data points. This fit is also consistent with that
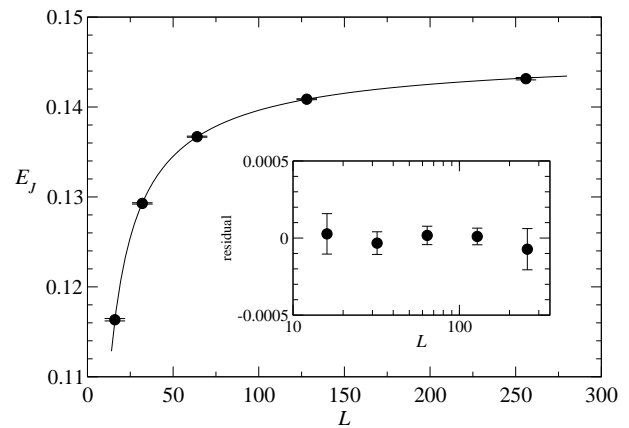


FIG. 26: A plot of $E_J$, the bond part of the energy density, for $h = 2.27$, as a function of $L$. The fit shown is of the form $E_J = c_1 - c_2 L^{(\alpha-1)/\nu}$, with $c_1 = 0.14632$, $c_2 = 0.29098$, and $(\alpha - 1)/\nu = -0.82$. The residuals (inset) give $\chi^2 = 0.65$. The statistical error in $(\alpha - 1)/\nu$ for fixed $h$ near $h_c$ is 0.02, but the uncertainty in this ratio is 0.10 due to the uncertainty in $h_c$.
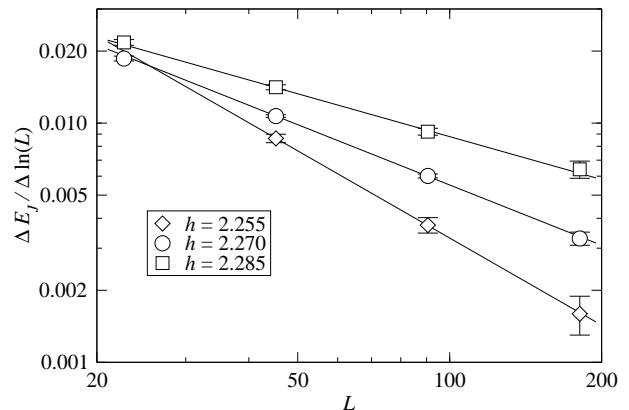


FIG. 27: Plots of the discrete derivative with respect to $\ln(L)$ of $E_J$, for $h = 2.255$, $2.270$, and $2.285$. The solid lines show power law fits for $L \geq 30$, with slopes 1.21, 0.84, and 0.60, respectively. Using the error estimate for $h_c$, this gives $(\alpha - 1)/\nu = -0.84 \pm 0.10$, consistent with the results from plots as in Fig. 26.

found from taking the derivative of $\overline{E}_J$ with respect to $\ln(L)$,

$$\frac{d\overline{E}_J}{d(\ln L)} \sim L^{(\alpha-1)/\nu}, \tag{55}$$

at $h = 2.27$, which removes the need to fit to $c_1$, but introduces larger uncertainties, due to the derivatives. This data for $h$ near $h_c$ is displayed in Fig. 27. By varying $h$ ($h = 2.255$, $2.280$), we estimate the systematic errors, given our uncertainty in $h_c$, arriving at the value $(\alpha - 1)/\nu = -0.82 \pm 0.10$, which, using $\nu = 1.37 \pm 0.09$, gives a second estimate $\alpha_{(2)} = -0.12 \pm 0.16$.

Besides the uncertainties in $h_c$, this result for $\alpha$ is affected by finite size corrections. We now argue that these

corrections can be reduced by extrapolation and that a connection exists between $\alpha$, $d_s^c$ and $\beta/\nu$: $E_J$, being the bond part of the energy density, is simply given by the density of domain walls, whose scaling can be found from the results in Sec. VIII. Namely, taking the surface area of clusters to scale with linear size $\ell$ as $A \sim \ell^{d_s^c} \sim v^{d_s^c/d}$ and using the constant limit for the distribution of volumes $\rho(v)d[\ln(v)]$ at large $v$, the domain wall density in a finite sample is found by integrating the wall density, taking into account intersections between the scales, over $L$ up to the system size, giving

$$\overline{E}_{J,s} \sim L^{d_s^c-d-\beta/\nu}. \tag{56}$$

This exponent can be justified by considering the change in $\overline{E}_{J,s}$ upon doubling the system size. With finite probability ($\rho_\infty \ln 2$), an extra domain wall of scale $L$ will be introduced. The connected surface of the domain wall will have area $L^{d_s^c}$, but the *increase in domain wall area* will be smaller, as the domain wall will intersect frozen regions. The fraction of the sample that is not frozen scales as $L^{-\beta/\nu}$ at criticality; the intersection of the new wall and the unfrozen region therefore scales as $\sim L^{d_s^c-\beta/\nu}$, so that the expected fraction of newly broken bonds (compared with the smaller sample) is $\sim L^{d_s^c-d-\beta/\nu}$. (The domain wall intersects frozen regions that did not have surfaces, as they were embedded in like spins, adding total area, and also intersects frozen clusters that had surface area, removing total area, but these contributions average to zero.) This argument implies the scaling relation

$$\frac{\alpha-1}{\nu} = d_s^c - d - \beta/\nu. \tag{57}$$

Note that this relation is consistent with modified hyperscaling, Eq. (6), and the conjectured relationships among the domain wall dimensions, Eqs. (43) and (52). Applying this result to our data, we find

$$(\alpha-1)/\nu = -0.74 \pm 0.02, \tag{58}$$

giving our best estimate

$$\alpha = -0.01 \pm 0.09. \tag{59}$$

Note that the magnitude of the $\beta/\nu$ contribution is small compared with the error.

Our result for $\alpha$ is in marked disagreement with the value from HY. The scaling assumptions for our and HY's analysis are identical. It may be that one set of results is more strongly affected by finite size errors, though we do fit larger values of $L$. We note that the value of $\alpha$ that we find using $E_J$ is extremely sensitive to the assumed value of $h_c$ and that the uncertainty in $h_c$ dominates the error estimate. A change of $h_c$ by $\delta h_c = 0.01$ gives a change $\delta[(\alpha-1)/\nu] \approx 0.2$ or $\delta\alpha \approx 0.3$. We are fitting for values near $h_c$, whereas the peaks in $C$ found by numerical differentiation are somewhat above $h_c$. In Sec. X, it is found that the convergence to a scaling function

for $h - h_c$ more than a couple of times $L^{-1/\nu}$, where the peaks in $C$ are, is slow compared with the convergence at $h = h_c$.

We use here two independent data sets to arrive at our estimates for $\alpha$: (a) total stiffness measurements on isotropic and anisotropic samples, with fixed BC's on two walls, applying finite size scaling, and (b) the measurements of the bond part of the total energy, $E_J$, using periodic isotropic samples, and fitting using a finite size scaling form. For (b), we analyze the samples in two ways: directly extracting $E_J$ data and also estimating the asymptotic scaling using the $d_s^c$ and $\beta/\nu$ measurements. This latter method is least sensitive to uncertainties in $h_c$.

### D. Deviations from criticality

As the system is taken away from the critical point, the nature of the spin clusters and correlations changes in a straightforward way. If the exchange is increased, driving the system into the ordered phase, then the large inverted droplets, which typically have gained energy of order $\ell^\theta$ at the critical point, will usually have this energy gain overcome by the extra exchange energy cost of order $\delta J \ell_J^d$ when $\ell$ is greater than the correlation length, $\xi$. Large inverted regions will be exponentially rare on length scales longer than $\xi$.

If the random field is increased or the exchange decreased to drive the system into the disordered phase, we can no longer simply focus on the inverted regions that already exist at the critical point but must also consider putative inverted regions that *could* exist. In any region with diameter of order $\ell$, there will be, at the critical point, an excitation that flips of order $\ell^d$ spins for a typical energy cost of order $\ell^\theta$ (more precisely it will only flip of order $\ell^{d-\beta/\nu}$ because of the frozen regions within it which are not sensitive to the boundary of the region). Since decreasing $J$ will decrease the energy cost of this excitation by an amount of order $\delta J L^{d_J}$, a good fraction of these "excitations" will have negative energy and thus occur spontaneously at scales of order $\xi$. On this and larger scales, the orientation of the spins will be determined primarily by the local random fields within a distance of order $\xi$ of the spins of interest.

### E. Thermal fluctuations and excitations

The effects of thermal fluctuations have been discussed elsewhere[2,48] in the general framework of a zero-temperature random field critical fixed point. We will thus restrict ourselves here to a few comments in light of the present more detailed picture.

At the critical point, as has been outlined above, there should be potential excitations with energy of order $\ell^\theta$ around each point, an independent one for roughly each factor of two in length scale, $\ell$. Since the energies of

these are random there is a finite probability density that the energy of any given one of them is near zero — indeed there would have been ones with negative energy but these give rise instead to the inverted clusters in the ground state. The thermal fluctuations are dominated by the *rare active excitations* whose energy is within of order $T$ of zero. Because $\theta$ is positive, the active excitations with diameters of order $\ell \gg 1$ occupy only a small fraction – of order $T/\ell^\theta$ – of the volume. But this small active fraction dominates the correlations, in particular causing the thermal fluctuations of the spin-spin correlations, the *truncated correlations*, to decay as

$$\overline{\langle (s_x - \langle s_x \rangle)(s_y - \langle s_y \rangle)\rangle} \sim \frac{T}{|x-y|^{d-2+\eta}} \qquad (60)$$

where the exponent $\eta$ is related to that of the zero-temperature correlations Eq. (48) by

$$\eta = \tilde{\eta} + \theta \qquad (61)$$

the extra factor of $T/|x-y|^\theta$ coming from the probability that both spins are in the same active excitation.[2]

In general, except for fluctuation quantities such as the truncated correlations, the statements that we have made about zero temperature will hold with minor (if sometimes subtle) modifications provided one considers always free energies instead of energies.

One effect which must be mentioned, however, is the "hypersensitivity" to changes along the critical line — sometimes, rather misleadingly, referred to as "chaos". As long as $\theta < d/2$, which we believe it probably is, although only barely so, which spins have which orientation at the critical point will depend, on sufficiently large scales, extremely sensitively on where one is on the critical line.[21,49] Unfortunately, due to the smallness of $d/2 - \theta$, this effect is unlikely to be observable in three dimensions but may be in higher dimensions for which $\theta$ is expected to deviate more significantly from $d/2$. (In six dimensions and above, $\theta = 2$.)

## X.  GROUND STATES AND SENSITIVITY TO BOUNDARY CONDITIONS

The simple picture of the random field Ising system exhibits two phases with a single transition between them: an ordered phase in which a typical spin is aligned with others far away; and a disordered phase in which the magnetization is zero and the orientation of each spin is determined locally by the random fields in its vicinity. In the ordered phase, $h < h_c$, spins have long range correlations and there are both "up" and "down" states, although domain walls can be introduced that divide the system into up and down regions. In contrast, when $h > h_c$, the spin correlation function is short ranged, with characteristic scale $\xi \sim (h - h_c)^{-\nu}$ and there is only one state; because of the locality, large scale domain walls do not exist in this phase.

But it is interesting to ask, by analogy with spin glasses and other systems with quenched randomness, whether the random field Ising system could be more complicated, especially near to the critical point. In order to address this, we must characterize the macroscopically distinct states in an infinite system: is there, as the simple picture would suggest, simply one state in the disordered phase and two in the ordered phase? Or is the behavior more subtle?

It has been claimed in the literature that "replica symmetry breaking" calculations show the existence of an intermediate glassy phase, where many solutions with distinct local magnetizations coexist for a finite range of parameter, between the paramagnetic and ferromagnetic phases.[7,8] But what does this mean? Indeed, what does one mean by "ground states" in an infinite system with random couplings? Furthermore, if one answers these questions, what is the connection between multiplicity of infinite system ground states and the notion of "replica symmetry breaking"?

To consider these questions, it is simplest to restrict consideration to systems, such as the RFIM with Gaussian random fields, in which the finite system ground states for given boundary conditions are non-degenerate with probability one. (Otherwise one gets into the complications of ground state entropy as in diluted antiferromagnets in a field and the bimodal RFIM;[50,51] but these issues are distinct from the basic questions of "states" on which we focus.)

### A.  Infinite system ground states

A *ground state of an infinite system* with finite range interactions is a configuration whose energy cannot be decreased by changing *any finite collection* of spins. Equivalently, a ground state can be thought of as the limit of a sequence of finite system ground states of larger and larger subsystems, generally with appropriately chosen boundary conditions on each size. Thus the set of all ground states for a specific infinite system, is the set of all distinct limits of sequences of boundary conditions.[31] For two ground states to be distinct, they must be distinguishable within some finite distance of the origin: if the finite system ground states differ only in regions whose distance from the origin grows without bound as the system size increases, then the infinite system ground states are the same.[52] All infinite system ground states have the *same energy density* but comparing the energy of a pair of ground states is not generally well-defined.

Many of the subtleties involved in considering infinite system ground states come to the fore in the ordered phase of the random field Ising model. If we take the limit of larger and larger systems with open (i.e. free) boundary conditions centered, for example, on the origin, then the finite system ground states will not approach a limit! This can be readily understood in terms of the "up" and "down" states which we know exist in the infinite system

– albeit with some finite density of misaligned spins.[1] A given finite sample of volume $\mathcal{V}$ will typically have random fields whose net effects are to cause an energy difference between the up and the down states which is of order $h\sqrt{\mathcal{V}}$. Thus the ground states with open boundary conditions will alternate randomly from mostly up to mostly down as a function of (the logarithm of the) system size. Of course, the up and down states can be found by either taking the appropriate subsequences with open boundary conditions, or by taking $+$ or $-$ boundary conditions on all sizes. The problem of energy comparison is now clear: which of these two states has the lower energy in a specific infinite system? This is manifestly ill-defined, indeed, because of the effects of the boundary conditions, it is not possible to uniquely define the energy of an infinite system ground state to higher accuracy than of order the surface area of the region under consideration.

We can, however, compare the energies of *some* pairs of infinite system ground states even in random systems. In high dimensions, greater than three, one can make ground states in the ordered phase of the RFIM with a domain wall that passes near the origin with a chosen orientation by putting $+$ boundary conditions on half of the boundary and $-$ on the other half. If the random fields are weak enough (in four and five dimensions, or with arbitrary randomness in the ordered phase in six or more dimensions), the domain wall will be flat on large scales with only *finite* typical deviations from planarity and its position and orientation can then be fixed by its intersection with the boundary which is forced by a "seam" between $+$ and $-$ areas of the boundary conditions. The infinite system domain wall state so constructed will be stable to changing any finite collection of spins, but, in a well-defined sense, it has higher energy than either the up or the down states. As the domain wall costs energy per unit area, if one looks at a sufficiently large region that overlaps the domain wall — say cubical with $v = \ell^d$ — the difference in energy between the domain wall state and the up state will be of order $J\ell^{d-1} \pm h\ell^{d/2}$ which is positive almost surely in the limit of large $\ell$.

In contrast to the higher dimensional case, in the three dimensional RFIM of primary interest, one *cannot* make infinite system domain wall states straightforwardly even in the ordered phase. If one tries to set up a domain wall that is, say, horizontal in a system of size $L \times L \times L$, one will find that the wall wanders in the vertical direction away from the plane determined by the boundary joint by a random, sample and subsystem size dependent amount of order $L^\zeta$ with $\zeta = 2/3$.[37,38,39] No matter how one adjusts the boundary seam, one is unlikely, in the large system limit, to be able to force the wall to be both near the origin and nearly horizontal. Thus the sequence of domain wall forcing boundary conditions will, in the ordered phase, contain one subsequence which converges to the up state, another which converges to the down state, and, almost surely, no other convergent subsequences. (There are subtleties, which we will not go into here, if

one allows a wall in the ordered phase to have *any* configuration dependent orientation; these will be addressed in Ref. 41.)

The crucial question that we would like to address here is whether there exists more than one infinite system ground state either at the critical point or slightly into the disordered phase. In principle, to investigate this one would need to study all possible sequences of boundary conditions, obviously an impractical task. In practice, one must restrict consideration to some small subset of boundary conditions and try to extract useful information about the infinite system limit by carefully studying the size dependence of various boundary conditions on regions near the origin.

## B. Numerical studies

We have studied how the ground state configurations change in response both to varying the boundary condition at fixed size and to changing the system size. We compare configurations for which the boundary spins are "open" ($O$), fixed positive ($+$), fixed negative ($-$), and random fixed spins ($R$). For fixed size calculations, for each realization of the random fields we compare all possible pairs of boundary conditions in the set $\{O, R, +, -\}$. We also compare ground state configurations for open boundary conditions on a sample of size $2L - 1$ (denoted $D$) that contains a subsample of size $L$, with the states for boundary conditions $O$, $+$ or $-$ imposed on the subsample. (The values of $L$ were taken to be odd for these comparisons, so that the origin coincides with a spin.) The results of all of the comparisons are characterized by counting how many spins differ for the two boundary conditions in a volume $w^3$ centered at the origin.

The primary emphasis of these calculations is to determine whether changes in boundary conditions can create configurations that differ from those with uniform $+$ or uniform $-$ boundary conditions, i.e., those that produce the up and the down states in the ordered phase. If the $+$ and the $-$ boundary conditions produce identical configurations in the deep interior, this suggests that there is only one state. If the probability that some other boundary condition produces a configuration in the interior that differs from those of *both* the the $+$ and $-$ boundary conditions, vanishes as $L \to \infty$, this suggests that there are at most two states.

We report here a selection of results for (a) the probabilities $P_{O\pm}(h, w, L)$ ($P_{R\pm}(h, w, L)$) that the boundary condition $O$ (respectively, $R$) gives a central volume $w^3$ that differs from that for *both* $+$ and $-$ boundary conditions at fixed sample size $L$; (b) the probability $P_{DO}(h, w, L)$ that the number of differing spins within the window is non-zero when one compares open boundary conditions for samples of size $2L - 1$ and a subsample of size $L$; and (c) the probability $P_{D\pm}(h, w, L)$ that open boundary conditions on the larger sample gives a central volume $w^3$ that differs from that for *both* $+$ and $-$

boundary conditions on the smaller sample.

The calculation of the probabilities $P_{O\pm}$ and $P_{R\pm}$ (comparisons (a)) allows us to study ground states near $h_c$. The events of interest are those where a given boundary condition $B$, either $B = R$ or $B = O$, gives a configuration distinct from both the $+$ and the $-$ boundary conditions. For $h > h_c$ as $L \to \infty$, $P_{B\pm}$ is expected to go to zero, since the effects of the boundary penetrate only a distance $O(\xi)$ into the sample. For $h < h_c$, in contrast, most of the interior configuration is either $+$ or $-$ and the chances that random or open boundaries yield some other possibility should again decay exponentially. At $h = h_c$, the correlation length diverges and at this critical point, we expect that the probability of a domain wall passing near the center decays only as a power of the system size. Using simple arguments based on the fractal nature of domain walls,[22,23] the probability that a window of size $w$ will intersect an object of fractal dimension $d_f$ scales as $(w/L)^{d-d_f}$. This is analogous to the probability of a domain wall in the ordered phase passing near the origin as discussed above. The appropriate fractal dimension to use here at the critical point is the dimension from box-counting, $d_I$, that we studied above. Basically, there is a substantial probability that open or random boundary conditions will, at the critical point, induce a system spanning domain wall relative to the $+$ and $-$ boundary conditions. Near the critical point, scaling suggests the form

$$P_{B\pm}(h, w, L) = L^{d_f - d} \mathcal{P}_B[w, (h - h_c)L^{-1/\nu}] \qquad (62)$$

for $B = R$ or $O$. We plot our data for $P_{O\pm}$, $w = 3$, in Fig. 28 and Fig. 29(a), assuming this scaling form, taking $h_c = 2.270$, $d_f = 2.25$ and the best fit value $\nu = 1.37$. The results for $P_{R\pm}$, while not shown here, are nearly identical, apparently converging for large $L$ near the critical point to an extremely similar, if not the same, scaling function, though the smaller $L$ curves have slightly different finite size corrections. We expect that $d_f$ is equal to the incongruent domain wall dimension $d_I$, as this is the domain wall dimension that describes changes in the bonds, and this expectation is consistent with our results.

We note that taking the value $d_f = 2.20$ appears to give a better fit for the peak heights away from $h_c$, but as convergence in several quantities is poorer away from $h_c$, the value $d_f = 2.25$ is acceptable. Directly fitting *the peaks* for $d_f$ gives a value $d_f = 2.22 \pm 0.03$.

The data for comparisons (a) should also scale with $w$ for large $w$: $\mathcal{P}[w, (h - h_c)L^{-1/\nu}] = w^{d-d_f}\mathcal{P}'[(h - h_c)L^{-1/\nu}]$. However, we do not have enough range in $w$ for $w >> 1$ to confirm this; for $w$ small, discreteness effects will prevent a collapse. For $L = 129$, the data do collapse well for $w = 65, 33, 15$, assuming the above scaling form and the best fit values of $h_c$, $d_I$, and $\nu$. Note that similar finite $w$ effects were also seen in the data of Ref. 22, where large $w$ was needed to see convergence to power law behavior in $w$, though scaling worked well for fixed $w$ with $L \gg 1$.

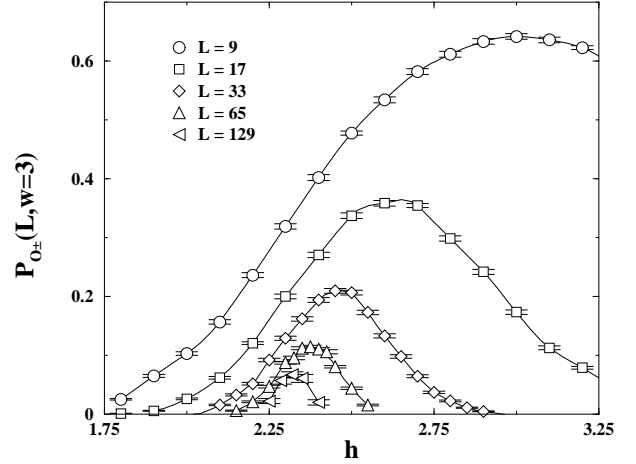Comparison (b) compares open boundary conditions



FIG. 28: Plot of the unscaled probability $P_{O\pm}$ that the central window of size $w = 3$ of a ground state configuration with open BCs on a given sample of size $L$, differs from the configuration in the window with *both* uniform $+$ and $-$ fixed boundary conditions. The lines are intended to organize the data visually.
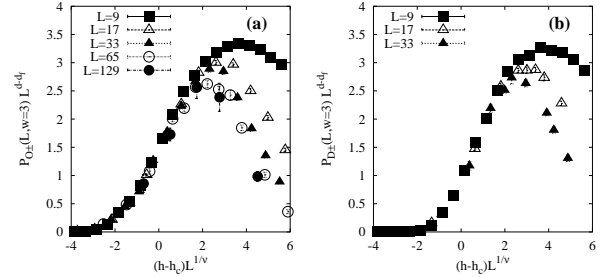


FIG. 29: Scaling plot for the probability that the central window of size $w = 3$ of a ground state configuration differs from that of uniform $+$ or $-$ fixed boundary conditions for (a) open boundary conditions on the same sample of size $L$ and (b) open boundary conditions on a sample of size $2L - 1$. The values used for scaling are $h_c = 2.270$, $\nu = 1.37$, and $d_f = 2.25$. The probabilities scale very well near $h = h_c$, but the peak heights, at $h > h_c$, converge slowly.

on two samples of different sizes, the smaller being a subsample of the larger centered at the origin. In the disordered phase, with the local spin configuration determined by the random fields nearby, doubling the size of the system is not expected to change the configuration in small windows near the origin, for $w \ll L$ and $L \gg \xi \sim (h - h_c)^{-\nu}$. But for $h < h_c$ and $L \gg \xi \sim (h_c - h)^{-\nu}$, the spin orientation is determined by the sign of the total (effective) random field which will depend stochastically on the system size as discussed in the previous subsection. For a fully magnetized system, ($|m| = 1$), these simple expectations yield $P_{DO} \to 0$ for

$L \to \infty$ with $w$ fixed for $h > h_c$, and

$$P_{DO} \to (7\pi^2)^{-1/2} \int_0^\infty dx \int_0^\infty dy \, e^{(-y^2/2 - (y+x)^2/14)}$$
(63)

for $h < h_c$ as $L \to \infty$. The integral in Eq. (63) is the probability that the total random field in the volume $(2L)^3$ exceeds in magnitude and is opposite in sign to the total random field in a subvolume $L^3$, assuming Gaussian distribution of the field on length scale $L$ with variance $L^3$. This integral gives a value $P_{DO} = 0.384973\ldots$ for $h < h_c$. The results of our ground state studies, displayed in Fig. 30, appear to be consistent with this limit, for $h < h_c$. This confirms the expectation that as the infinite volume limit is taken in the ordered phase, the spins in a fixed volume flip between two distinct configurations infinitely often — typically every factor of three or so in length scale. Near the critical point, the probability of differences in the window between the full and the subsample will be modified since with $|m| < 1$, there is a non-zero probability that the window will be contained in a frozen spin clusters that is unaffected by the overall majority random field. But this $w$-dependent difference only becomes important near $h_c$, as $\beta$ is so small.

Right at the critical point the effects of frozen clusters on all scales should in principle suppress $P_{DO}$ to zero in the large $L$ limit for all $w$; but as it will decay only as $1/L^{\beta/\nu}$, this effect is hard to see. In the disordered phase, our data is consistent with $P_{DO}$ vanishing exponentially for $L \gg \xi$.

Comparison (c) allows us to address nearly the same question as (a), but more directly checks that increasing the volume of the system has the effect of setting an effective boundary condition of $+$ or $-$ on the central region. The scaling collapse, shown in Fig. 29(b) is acceptable, as it is in (a), with a scaling function similar to, but distinct from that for comparison (a). The results for $P_{D\pm}$ show that, except for a region near $h_c$ that shrinks and decreases in probability with increasing $L$, the configuration given by the larger system with open boundary conditions does *not* produce a distinct interior volume from that found by imposing $+$ or $-$ boundary conditions on the smaller system of size $L$.

Taken together, these results are consistent with the expectations from the simple scenario for the structure of the states given above; there do not seem to be any indications of stranger behavior. Thus, in the absence of concrete testable predictions from those who believe there should be more than just the simple set of states, we can do no more than conclude that if they can indeed occur, it must be only under very subtle conditions.

## XI. SUMMARY

In this paper, we have presented numerical results for the ground states of 3D random field Ising magnets focusing on the transition between the ordered and disordered phases. Our results allow us to conclude that the
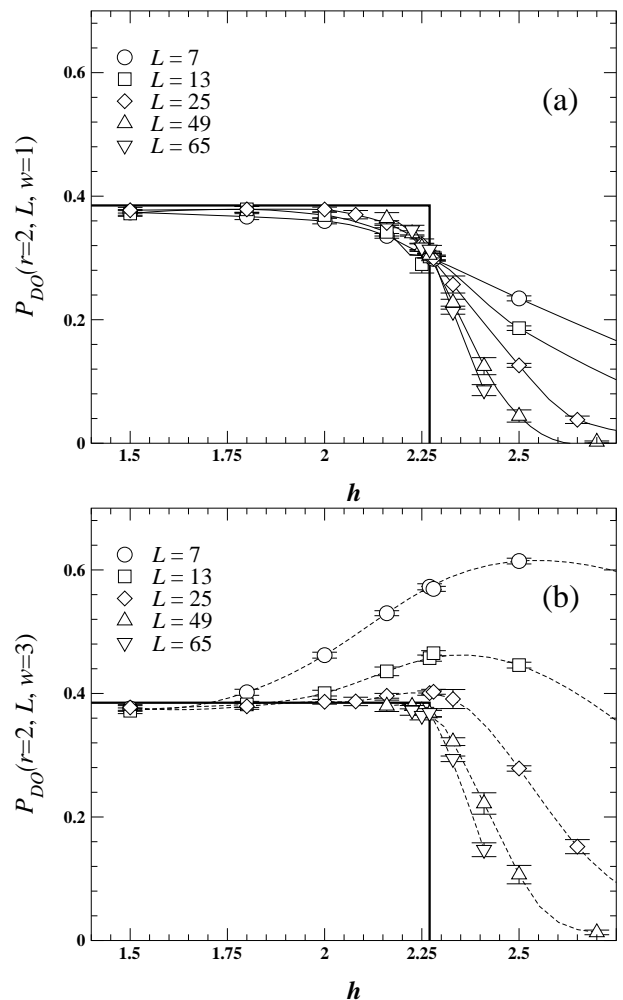


FIG. 30: Probability $P_{DO}$ that the central window of size (a) $w = 1$ and (b) $w = 3$ of a ground state configuration in a subsample of size $L$ differs from that in a sample of size $2L-1$, with open boundary conditions on the subsample and sample. Note that the sample sizes are approximately separated by a factor of 2, except for the largest two sizes. For small $h$, the probability $P_{DO} \approx 0.38$, quantitatively consistent with a simple model with two states. For large $h$, $P_{DO} \to 0$ as $L \to \infty$, consistent with a single state. The solid line shows the step function that would obtain for $P_{DO}$ in the $\infty$-volume (and large $w$) limit, *if* it were the case that $|m| \equiv 1$ in the ferromagnetic phase, taking $h_c = 2.270$. The data is consistent with the calculated $P_{DO}$ values approaching this step function at larger sizes $L$, for $h \neq h_c$. Note that at $h = h_c$, $P_{DO} \approx 0.368 \pm 0.006 < 0.379\ldots$ for $L = 97$ and $L = 129$, $w = 3$, consistent with a constant or slowly decaying value of $P_{DO}$ at the critical point. The dashed curves are spline fits to organize the data visually.

transition is second order, though the magnitude of the magnetization vanishes very slowly as the critical random field strength, $h_c$, is approached from below. In addition to the magnetization, we have studied the stiffness of the system and some of the geometrical aspects, in particular the fractal properties of domain walls at the critical

point. In general, the results agree very well with a scaling picture of the transition introduced some time ago[2] and extensions of it to the properties studied here.

Some earlier authors have suggested that the behavior of the RFIM near to the ordering transition will be more complicated than this scenario, arguing for some kind of "replica symmetry breaking". Although, as is so often the case, the meaning of this term in this context has not been made clear, if we take it to imply the existence of many infinite volume ground states, this would have testable consequences. Although a full test of the dependence of the ground states on sequences of boundary conditions that this would imply is beyond the scope of today's computers and algorithms, we have made some preliminary tests on the dependence on boundary conditions. In particular, we have studied the probability that the configuration in a fixed volume at the center of a sample can be induced to differ from both the fixed $s = +1$ and fixed $s = -1$ boundary conditions by various other boundary conditions. With the range of boundary conditions we have tested, this probability vanishes in the expected manner as $L \to \infty$. Indeed, the power law dependence of this probability on $L$ and the scaling with $h - h_c$ are consistent with the domain wall fractal dimension and correlation length exponents determined by other methods. Our results are thus consistent with a single disordered to ordered transition at $h_c$, with a unique state in the disordered phases and a pair of states ("up" and "down") in the ordered phase. Recent simulations at finite temperature in smaller systems by Sinova and Canright,[53] who used the spectrum of the spin-spin correlation matrix and $P(q)$ distributions, also suggest a single transition.

At non-zero temperature, the thermodynamic properties of the phase transition are believed to be similar to those at zero temperature: the transition is governed by a *zero temperature fixed point*. But at positive temperature, one can also consider dynamic effects; indeed, as has been known for a long time, these dominate both Monte Carlo simulations and experiments. As first pointed out by Griffiths,[54] random systems can have singularities — albeit very weak ones — in thermodynamic properties well before the transition is reached and this will be the case for the RFIM. These rare region effects are unobservable as far as equilibrium properties in classical systems, but do have dynamic consequences.[55,56,57] In the Griffiths region above the transition, the average dynamic autocorrelations will decay more slowly than exponentially because of the effects of anomalously ordered local regions. Perhaps this kind of rare-region effect, and the more interesting but related effects that occur as the transition is approached, are all that is meant by "replica symmetry breaking". If this is the case, then it would be nice if the proponents of these ideas would say so. If not, then it is incumbent upon them to come up with some testable predictions. If these can be tested by static ground state properties, the RFIM is as good as system as any on which to perform such tests as the system sizes

that can be studied are quite impressive: comparable to the largest that can be studied by Monte Carlo simulations in pure systems.

## APPENDIX A: ALGORITHM IMPLEMENTATION

We briefly describe here the algorithm and code used, including modifications to the conventional RFIM max-flow problem; outline the verification procedure for the code; and briefly outline the statistics and error bar procedure.

### 1. Base code and modifications

There is a now well-known mapping of the RFIM ground state problem to a min-cut/max-flow problem.[14] This correspondence and the push-relabel algorithm for the max-flow problem, including terms used here (such as layers and excesses), is well described in reviews and texts, such as Refs. 18, 58, and 16. The implementation of the Goldberg-Tarjan[59] max-flow algorithm that we started with was the h_prf code in C written by Cherkassky and Goldberg,[15] which in general performs quite well for a number of graph topologies.

We modified the code to be more compatible with the C++ language and developed objects (including samples, configuration subsets as windows, and random number generators) to conveniently implement a variety of boundary conditions and analyses. One very simple benefit of an integrated code is that the graph input, which is quite costly when read as a text file, is greatly sped up. More importantly, the short main routine was easily modified to compute answers to a wide number of questions.

The most significant change to the core push-relabel code was a modification that allowed for positive and negative excesses. This modification was developed in collaboration with D. McNamara.[60] The central idea is the elimination of the source and sink nodes, which conventionally have links to the nodes of the graph representing the spins $s_i$, in favor of introducing nodes with a negative excess. The first step in the conventional algorithm pushes as much flow as possible from the source

onto the lattice nodes. This step is replaced in our code with an initialization where a positive excess $h_i$ is placed on each node for which $h_i > 0$. The connections to the sink are substituted for by placing a *negative* excess on the nodes with $h_i < 0$. The push-relabel algorithm then proceeds with the usual steps, with the nodes with positive excess having their excess pushed and their heights relabeled, as appropriate. The negative excess nodes act as sinks for the positive excess, until such a nodes total excess becomes positive. Besides removing the links to the source and sink, the global relabeling step must be modified. Instead of carrying out a breadth first search from the sink node, the breadth first search instead starts from the nodes with negative excess. (If no negative excess nodes remain, the algorithm terminates with flow equal to the sum of the positive $h_i$.) The initial totals of the positive and the negative excesses are compared with the final totals: the decrease in the total positive flow, for example, gives the maximum flow through the graph. The spin configuration and magnetization is determined by counting the number of nodes that are in the maximal layer.

The removal of the source and sink nodes reduces the amount of memory used by an amount $1/(d+1)$ relative to the conventional memory requirements and results in a slight speedup. For the largest lattice sizes studied ($256^3$), memory requirements were reduced at the cost of speed. If pointers and integers each require 4 bytes, the Cherkassky and Goldberg implementation requires 16 bytes for each arc and 32 bytes for each node (counting the layers as part of the per-node requirements.) The use of pointers was retained for system sizes up to $128^3$. For a regular lattice, however, the nodes at the end of each arc, sister arcs, and the list of arcs at each node can be recomputed whenever needed. For a cubic lattice, then, the number of bytes per node is reduced from $(6 \times 16 + 32) = 128$ bytes to $(6 \times 4 + 32) = 56$ bytes. For $L^3 = 128^3$ samples, the running time increased by a factor of $\approx 2.5$, primarily due to the recomputation of the tail nodes of the arcs and the sister arcs.

One modification for the $256^3$ samples was made that is not strictly sound, in that the algorithm could conceivably fail. In order to save memory, a limit to the maximum number of layers was implemented. In the Cherkassky and Goldberg code, the number of layers allocated is given by the number of nodes in the graph. In practice, however, far fewer are needed. A check over 1000 samples for $8 < L < 128$ was carried out, for several values of $h$. The number of layers needed, $K$, appears to be largest for $h \approx h_c$. At this value, the sample mean of the maximum layer needed is about $\overline{K} \approx 2L$. The distribution over samples of the number of layers needed roughly scales with $L$, though the dependence of the width of the distribution could be $L^x$, with $x$ near 1. In any case, the distribution drops off very quickly with $K$. The maximum number of layers needed over 1000 samples scales roughly linearly with $L$, $K^{\max} \approx 7L$, where the maximum is for periodic boundary conditions and

over a range of $h$, $2.0 < h < 2.5$, with a peak in $K^{\max}(h)$ near $h_c \approx 2.27$ (though the peak is slightly above $h_c$ for smaller samples.) The mean number of layers fits relatively well to a scaling collapse, with a maximum value scaling consistent with $L^{1.08}$ (or even $L\sqrt{\ln L}$), scaling about $h_c \approx 2.27$ with $\nu \approx 1.35$. We set $5 \times 10^4$ as the maximum number of layers for all sample sizes, which is nearly $200 \times L$ for the largest samples studied. This number of layers was easily sufficient for all samples studied. The amount of memory needed for cubic lattices is then $48 + O(L^{-2})$ bytes per node.

## 2. Verification

The modifications made to the base code, while theoretically sound (except for the limit on the number of layers), could inadvertently introduce errors, due to errors in coding. We therefore verified the code against the Cherkassky and Goldberg codes h_prf and hi_pr (version 3.3) codes[15,61] and a selection of other codes that were not based on a push-relabel algorithm. This was done by having the production code write out the list of the $h_i$. A small program then converted these $h_i$ into arcs and nodes into a graph description DIMACS format, using the conventional representation with a source and a sink.

These graph descriptions were then used as input to h_prf, hi_pr, and other codes, such as those developed in the First DIMACS Challenge.[62] The flows and the magnetization from these available algorithms were then compared, sample by sample, with the production code. The precise comparison was done for a few tens of samples with ferromagnetic coupling strength $J = 10, 10^2, \ldots, 10^7$, relative disorder strength $h/J = 1, 2.3, 3, 10$ and system sizes $L = 4, 8, \ldots, 128$. The production code and the other algorithms agreed in all cases, except when the flow exceeded $2^{31}$, which was generally the maximum possible flow in the available algorithms. The production code used here does not have that restriction, as flow computation is done at the end by comparing the initial and final positive and negative excesses, which were summed up as double precision quantities. The code was able to handle larger flows consistently, as could be verified by scaling $h$ and $J$ to large values (multiplying $J$ and the $h_i$ by a factor of, say, $10^5$, and checking that the maximum flow increases proportionately and that the configuration is unchanged.)

For efficiency, we have used an integer algorithm, with a resolution of $10^4$ by replacing the $h_i$ by random integers found by rounding $z_i \times 10^4$ towards zero, with $z_i$ Gaussian random variables with zero mean and unit variance and the exchange by $J/h \times 10^4$. We checked that *reducing* this resolution by a factor of 10 for selected measurements did not affect the computed averages, such as the stiffness in the isotropic and anisotropic samples for systems up to $128^3$. For a resolution of $10^2$, there were discrepancies outside of statistical errors, but these discrepancies could be consistently explained by the effects of rounding to an
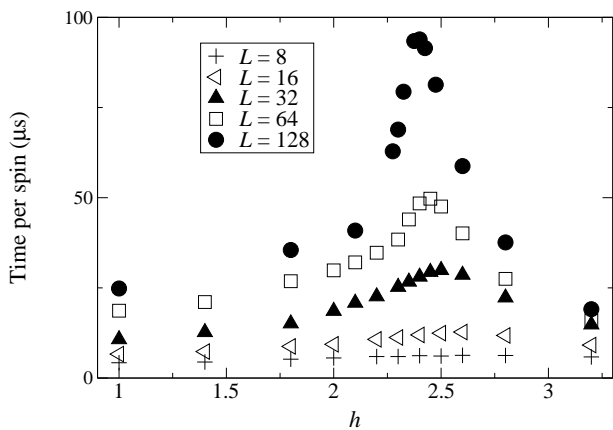
FIG. 31: Elapsed time for computing ground states in the RFIM, plotted vs. $h$, for linear sizes $L = 8, 16, \ldots, 128$. The "fast" algorithm is applied, with the larger memory requirements, on a 766 MHz Pentium III processor. The peak times *per spin* scales nearly linearly with $L$.

integer, which shifts the width of the distribution of $h_i$ by a small, predictable amount.

We also tested the assumption that the cut found was unique (that is, that the ground state was unique, for a given sample.) Some accidental degeneracies were found, at the level of a fraction of spins $\approx 0.9 \times 10^{-6}$, for $h$ near 2, including $h_c$. This would result in the magnetizations being in error at the level of $< 10^{-6}$, well within the statistical errors. Increasing the resolution by a factor of 10 increases the running time by about 7% and reduces the fraction of degenerate spins to $\approx 2 \times 10^{-7}$. As the degeneracies were for the most part attributable to single spins, were rare, and did not affect any of the sample averaged results in the cases we tested, the integer scale of $10^4$ was more than sufficient for this study.

We have verified that our choice of random number generator does not affect the results. Specifically, we used two generators for the computations of the magnetization and domains (defined in Sec. VIII) in $256^3$ samples at $h = 2.27 \approx h_c$ and found the results to agree within statistical errors (the results reported pool the results from these generators.) We also checked the results from the two generators against each other for a larger number of smaller systems.

Though quantities computed and the details of our interpretation differ from previous work, the numerical values for the same sample sizes and measurements (for example, magnetization and the largest cluster sizes) are consistent with published data.[11,44]

### 3. Timing

Consistent with similar optimization problems related to physical problems, the typical CPU time needed to

find the ground state scales roughly as $N^{1.3}$ near $h_c$. Roughly, it takes about 16-20 times longer to find the
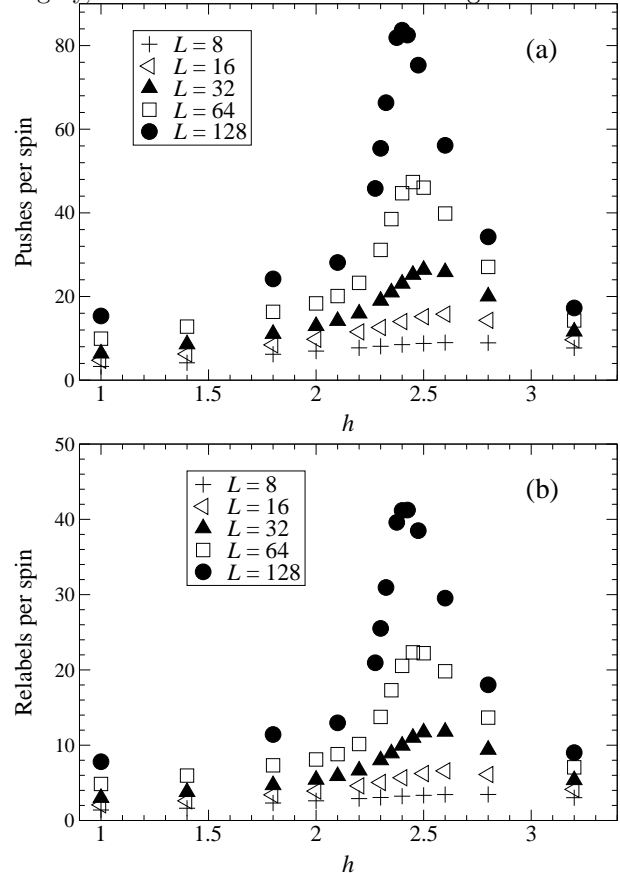


FIG. 32: Statistics for the "operations", pushes (a) and relabels (b), performed in computing ground states in the RFIM, plotted vs. $h$, for linear sizes $L = 8, 16, \ldots, 128$. The peak number of operations *per spin* scales nearly linearly with $L$ (near $h_c$). At both high and low $h$, the number of these rearrangements scales nearly as $L^{0.3}$.

ground state each time the sample size is doubled, for $h \approx h_c$. Using CC on a 400 MHz Sun UltraSparc II (the San Diego Supercomputing Center Sun HDSC10000), a $256^3$ lattice required 913 MB of memory total for the graph data, the instructions, and the data structures required for analysis. Running time for this size and this architecture averaged 1.8 hours per sample, for $h = 2.27$. Run times, normalized to the elapsed time per spin, for the larger memory algorithm, with the full data structure, are plotted in Fig. 31. Clearly, the shape of the elapsed time vs. $h$ sharpens some as $L$ increases. The peak running time scales as $\sim L^{4.0}$ over the scales $L = 8$ to $L = 128$. Further details of the scaling of the running time and connections between the algorithm and the physical concepts of ground state degeneracy and correlation length are described in Ref.63.

[1] J. Z. Imbrie, Phys. Rev. Lett. **53**, 1747 (1984); Comm. Math. Phys. **98**, 145 (1985). J. Bricmont and A. Kupiainen, Phys. Rev. Lett. **59**, 1829 (1987).

[2] D. S. Fisher, Phys. Rev. Lett. **56**, 416 (1986).

[3] J. Villain, Phys. Rev. Lett. 52, 1543 (1984).

[4] A. T. Ogielski, Phys. Rev. Lett. **57**, 1251 (1986).

[5] J. C. Anglès d'Auriac and N. Sourlas, Europhys. Lett. **39**, 473 (1997).

[6] N. Sourlas, Comp. Phys. Comm. **121**, 184 (1999).

[7] M. Mézard and A.P. Young, Europhys. Lett. **18**, 653 (1992).

[8] M. Mézard and R. Monasson, Phys. Rev. B **50**, 7199 (1994).

[9] T. Nattermann in "Spin Glasses and Random Fields", ed. A. P. Young (World Scientific, Singapore, 1998).

[10] M. R. Swift, A. J. Bray, A. Maritan, M. Cieplak, and J. R. Banavar, Europhys. Lett. **38**, 273 (1997).

[11] A. K. Hartmann and U. Nowak, Eur. Phys. J. B **7**, 105 (1999).

[12] H. Rieger, Phys. Rev. B **52**, 6659 (1995).

[13] J. Machta, M. E. J. Newman, and L. B. Chayes, Phys. Rev. E **62**, 8782 (2000).

[14] J. C. A. d'Auriac, M. Preissmann, and R. Rammal, J. Phys. Lett. **46**, L173 (1985).

[15] B. Cherkassky and A. Goldberg, Algorithmica **19**, 390 (1997).

[16] *Introduction To Algorithms*, T. H. Cormen, C. E. Leiserson, and R. L. Rivest (MIT Press, Cambridge, Massachusetts, 1990).

[17] A. A. Middleton, Phys. Rev. E **52**, 3337 (1995).

[18] See, e.g., H. Rieger, Lecture Notes in Physics 501 (Springer-Verlag, Heidelberg, 1998).

[19] W. L. McMillan, Phys. Rev. B **30**, 476 (1984).

[20] A. J. Bray and M. A. Moore, Phys. Rev. B **31**, 631 (1985).

[21] A. J. Bray and M. A. Moore, Phys. Rev. Lett. **58**, 57 (1987).

[22] A. A. Middleton, Phys. Rev. Lett. **83**, 1672 (1999).

[23] M. Palassini and A. P. Young, Phys. Rev. B **60**, 9919 (1999).

[24] M. Palassini and A. P. Young, Phys. Rev. Lett. **83**, 5126 (1999).

[25] For the similar case of the ferromagnetic to spin glass transition in two dimensions, see the numerical work of W. L. McMillan, Phys. Rev. B 29, 4026 (1984).

[26] A. K. Hartmann and P. Young, cond-mat/0105310.

[27] D. P. Belanger, A. R. King, V. Jaccarino, and J. L. Cardy, Phys. Rev. B **28**, 2522 (1983).

[28] The data is well fit assuming a simple correction to scaling with $\rho(v) = \rho_\infty + bv^{-y}$, with $\rho_\infty = 0.0019$, to within $10^{-4}$, $b$ a fitted constant, and $y$ on the order of 0.4. The principle uncertainty in $\rho_\infty$ comes from the uncertainty in $h_c$: the value to which $\rho(v)$ converges would vary if $h_c$ is slightly greater or smaller than 2.27, as is apparent in Fig. 25.

[29] D. J. Thouless, Phys. Rev. **187**, 732 (1969); M. Aizenmann, J. Chayes, L. Chayes, C. Newman, J. Stat. Phys. **50**, 1 (1988).

[30] M. S. Cao and J. Machta, Phys. Rev. B **48**, 3177 (1993).

[31] C. M. Newman and D. L. Stein, Phys. Rev. B **46**, 973 (1992); Phys. Rev. Lett. **72**, 2286 (1994); **76**, 515 (1996); **76**, 4821 (1996); Phys. Rev. E **55**, 5194 (1997); **57**, 1356 (1998).

[32] D. A. Huse and D. S. Fisher, J. Phys. A **20**, L997 (1987); D. S. Fisher and D. A. Huse, J. Phys. A **20**, L1005 (1987).

[33] M. Schwartz and A. Soffer, Phys. Rev. Lett. **55**, 2499 (1985).

[34] Y. Imry and S. Ma, Phys. Rev. Lett. **35**, 1399 (1975).

[35] E. Brézin and C. De Dominicis, arXiv:cond-mat/0007457.

[36] J. T. Chayes, L. Chayes, D. S. Fisher, and T. Spencer, Phys. Rev. Lett. **57**, 2999 (1986); Comm. Math. Phys. 120, 501 (1989).

[37] G. Grinstein and S. K. Ma, Phys. Rev. B **28**, 2588 (1983).

[38] D. A. Huse and C. L. Henley, Phys. Rev. Lett. **54**, 2708 (1985).

[39] D. S. Fisher, Phys. Rev. Lett. **56**, 1964 (1986).

[40] P. Chauve, P. Le Doussal, K. Wiese, Phys. Rev. Lett. 86, 1785 (2001).

[41] A. A. Middleton, unpublished.

[42] J. L. Cardy, J. Phys. A **17**, L385 (1984).

[43] J. Shao and D. Tu, *The Jackknife and Bootstrap* (Springer-Verlag, New York, 1995).

[44] J. Esser, U. Nowak, and K. D. Usadel, Phys. Rev. B **55**, 5866 (1997).

[45] The level of nesting of domains at $h_c$ varies with system size. For $L = 32$, 95% of the samples had minority spin clusters, but these had no subclusters; in the remaining 5% the depth $k = 2$: minority clusters had majority spin inclusions. Out of the $64^3$ samples, 51% had $k = 1$ and 49% had $k = 2$. About 0.1% of the $128^3$ samples had depth $k = 3$, 1.7% had $k = 1$, with the remainder having $k = 2$. The $256^3$ samples had the highest nesting, though as $\beta/\nu$ is small, the nesting is still relatively small: 10 samples out of 1000, or about 1%, had $k = 3$, 989 had a depth of 2 and 1 had $k = 1$.

[46] J. L. Cardy, J. Phys. A **17**, L961 (1984).

[47] H. Rieger and A. P. Young, J. Phys. A **26**, 5279 (1993).

[48] D. S. Fisher, J. App. Phy. **61**, 3672 (1987).

[49] M. Alava and H. Rieger, Phys. Rev. E **58**, 4284 (1998).

[50] S. Bastea and P. M. Duxbury, Phys. Rev. E **58**, 4261 (1998).

[51] A. Hartmann, Physica A **248**, 1 (1998).

[52] D. Newman and C. Stein, cond-mat/0103616.

[53] J. Sinova and G. Canright, cond-mat/0103071.

[54] R. B. Griffiths, Phys. Rev. Lett. **23**, 17 (1969).

[55] M. Randeria, J. P. Sethna, and R. G. Palmer, Phys. Rev. Lett. **54**, 1321 (1985).

[56] D. Dhar, M. Randeria, and J. P. Sethna, Europhys. Lett. **5**, 485 (1988).

[57] D. A. Huse and D. S. Fisher, Phys. Rev. B **35**, 6841 (1987).

[58] M.J. Alava, P.M. Duxbury, C. Moukarzel and H. Rieger, *Exact combinatorial algorithms: Ground states of disordered systems*, For Domb and Lebowitz series, in press.

[59] A. V. Goldberg and R. E. Tarjan, J. ACM **35**, 921 (1988).

[60] D. L. McNamara, Ph.D. thesis, Syracuse University (1999).

[61] This code currently can be found at http://www.star-lab.com/goldberg/index.html.

[62] *Network Flows and Matching: First DIMACS Implementation Challenge*, David S. Johnson and Catherine C. McGeoch, eds (American Mathematical Society, Providence, RI, 1993.) Also see ftp://dimacs.rutgers.edu/pub/netflow.

[63] A. A. Middleton, cond-mat/0104185.